Glider-Based O$_2$ and CO$_2$ Observations in the Labrador Sea

by

© Nicolai von Oppeln-Bronikowski

A thesis submitted to the School of Graduate Studies

in partial fulfilment of the requirements for the degree of

Master of Science

Department of Physics and Physical Oceanography

Memorial University of Newfoundland

May 2019

St. John's   Newfoundland

Abstract

Ocean gliders can provide high-resolution gas observations necessary to interpret the space and time scales of highly dynamic processes such as gas uptake or outgassing in the ocean surface layer. There is a critical need to make high-resolution in situ gas measurements in the ocean for the biogeochemical community (Johnson et al., 2009). Small optical sensor, called optodes, have been used on gliders to measure dissolved oxygen in the oceans and recently optodes were modified to measure pCO_2 (Atamanchuk et al., 2014). The CO_2 optode is in an early prototype stage and has not undergone rigorous testing on a glider. Here we describe our approach to reference glider based O_2 and pCO_2 measurements to data from a vertical profiler mooring – the SeaCycler to validate the glider data. The SeaCycler carried a Pro-Oceanus Ltd., CO_2-Pro CV as part of its instrument float, an extensively tested gas analyzer, based on non-dispersive infrared refraction (NDIR), which has shown stable performance during lengthy observations (Jiang et al., 2014). We compare the glider data against the SeaCycler's O_2 and CO_2 measurements to compute an isopycnal-matched in-situ optode correction. We conducted further glider tests of the sensor on the Newfoundland Shelf in 2018 and further characterized the response time in profiling applications. In this thesis, we show data from both deployments to characterize the sensor performance. We discuss the spatial and temporal structure in the Labrador Sea glider data and use frequency and correlation length scale analysis to infer the presence of short internal wave energies near the buoyancy frequency range. From the results of the glider missions, we present ideas to improve future glider missions into the Labrador Sea and glider based CO_2 measurements.

Acknowledgements

Contents

List of Figures

Chapter 1

Introduction

1.1   Motivation for this Thesis

The motivation of this work starts with the Ocean Observing Conference of 2009 at which the global biogeochemical community asked the autonomous sampling teams across the world to advance remote sampling of CO_2 parameters in the global ocean environment. CO_2 is a critical parameter in the atmosphere and the ocean, intrinsically linked to the biological and physical processes that have shaped our planet in the past and will in the future. Since Ocean Obs'09, several projects, improving the understanding of the strength of oceanic CO_2 uptake sinks, such as the Surface Ocean CO_2 Atlas (SOCAT) have been made possible by community efforts to reach standards for mobile in-situ sampling technology. However, there is still a lack of regular high-resolution measurements of oceanic CO_2 system parameters in most of the world's ocean regions. Intense carbon uptake, associated with regions of energetic atmospheric heat exchange such as the Labrador Sea, has raised alarming questions

about the future role of these regions during times of global climate change. Depth-resolved carbon measurements are a necessity.

Through combined national and international scientific efforts, a dedicated research program was funded through the National Science and Engineering Research Council (NSERC), Climate Change and Atmospheric Research (CCAR) network to observe and study the Labrador Sea: Ventilations, Interactions and Transport Across the Labrador Sea (VITALS) program. This program, which encompassed modelling and observational components worked together across scientific disciplines with on-going Canadian and international research efforts to implement a holistic plan to measure some of the short time scale processes of carbon uptake and lateral exchange in the Labrador Sea. This thesis examines the results of the deployment of a glider and vertical profiler – the SeaCycler, in the Labrador Sea. We present the data and our analysis and discussion around central themed questions:

- How to measure CO_2 using gliders in the open ocean?

- How can multiple autonomous platforms be used to help improve sensor data?

- How to best observe spatial and temporal structure with gliders in the Labrador Sea?

Answering these questions is critical, to improve and shape our current and future plans for carbon observing systems utilizing glider and other platforms, especially as new technology is being developed such as new CO_2 or pH sensors. We also present new observations of fall conditions in the Labrador Sea, a very dynamic ocean frontier.

1.2 Marine CO_2 and Carbon Observing Needs

The global ocean system plays a crucial role in absorbing the effects of changes to the Earth's atmospheric composition due to anthropogenic activities. Roughly one-third of all anthropogenic CO_2 (C_{ant}) released into the atmosphere since the beginning of the industrial revolution has been taken up by the ocean, a total of 155 ± 31 PgC as of 2010 (Khatiwala et al., 2013). Increased CO_2 levels are directly linked to an increase in free hydrogen ions causing a decrease in pH, at a rate of change that is faster than any time in the past geological record (Zeebe et al., 2016). This decrease in pH, termed ocean acidification (OA), causes detrimental effects on marine habitats by disrupting carbonate mineral saturation states affecting, for example, the growth of corals (Cohen and Holcomb, 2009; Guinotte and Fabry, 2009).

The uptake of CO_2, however, does not happen equally in the ocean, as colder surface waters in northern and southern latitudes have higher CO_2 solubility (Volk and Hoffert, 1985). Key oceanic sites in the world act as global carbon sinks also termed solubility pumps, such as the Labrador Sea (DeGrandpre et al., 2006) and the Weddell Sea (van Heuven et al., 2014). These sites undergo deep vertical mixing in the wintertime bringing atmospheric CO_2 to deep water mass transports such as the Atlantic Meridional Overturning Circulation (AMOC) through which carbon can spread to the rest of the world's ocean (Broecker, 1991; Fontela et al., 2016). In addition to these physical processes, plankton and bacteria contribute to top layer biological pumping of oxygen and carbon dioxide through uptake and respiration which increases the carbon content in the upper water column before convection takes place (Azetsu-Scott et al., 2010). Linking the global ocean system to the carbon

uptake in these regions must be studied to assess the rate of OA. There is a critical need for a global ocean carbon measurement system because existing observations are limited in coverage and quality (Borges et al., 2010; Okazaki et al., 2017). Some are calling on recent advances in autonomous sampling strategies, such as ocean gliders (Rudnick, 2016), to form a biogeochemical observing network (Johnson et al., 2009).

1.3   The VITALS Program

Advancing autonomous measurements of critical biogeochemical variables such as CO_2, are complicated by technology, data quality and logistical challenges around organizing scientific observing programs. Yet, we cannot delay new observations until a perfect solution is achieved, as time and spatial scales of carbon-ocean dynamics are impacted by anthropogenic climate change. Nor do we believe autonomous in-situ sampling capabilities will be improved without deploying current state-of-the-art technology and accepting a certain element of risks associated with pioneering missions.

A key ocean region connected to the widespread impact of increased anthropogenic carbon emissions into the atmosphere is the Labrador Sea. The confluence of different water mass transports, contrasting freshwater influx and atmospheric forcing, leads to large interannual variations of ocean dynamics on all scales, focused in a comparatively small ocean region. This makes the Labrador Sea a challenging and vital ocean basin for the physical-biogeochemical sciences (Körtzinger et al., 2004; Kieke et al., 2007; Yashayaev and Loder, 2009). The important work and data amassed over decades through direct observations, modelling and reanalysis, have put the Labrador

Sea in prime focus as a regulator of deep ocean carbon content (Sabine et al., 2004; Sabine and Tanhua, 2010). As part of the VITALS project, we devised an observing strategy to carry out novel in-situ observations to:

- Reach the deep convection region with a glider to carry out sampling with the novel foil-based pCO_2 sensor from Aanderaa with minimal ship resources for launch and recovery

- Use measurements provided by the autonomous SeaCycler profiler carrying the larger payload CO_2-Pro CV instrument for glider in-situ calibration points.

This mission presents one of the first attempts to use a moored sensing platform as an in-situ reference point for experimental sensors deployed on a glider to advance data quality and coherence of novel biogeochemical measurements. This is an important step towards increasing the spatial and temporal coverage of oceanic carbon measurements as technology is playing a catch-up game. We extended this mission in September 2018 on the Newfoundland Shelf, in Trinity Bay, to further test the concept, flying the glider near a small fishing boat from which reference casts were taken using the same Pro CV instrument. We utilize these two real ocean deployments to improve sensor characterization and the quality of the collected data.

1.4   Chapter Overview

This thesis is composed of six chapters, with a comprehensive background review, Chapter 2 summarizes the standard oceanographic and geographic role of the Labrador Sea region. This section also reviews theory on CO_2 uptake, storage and exchange

to present a good basis for the remaining chapters. We also introduce available sensing technology for CO_2, and past glider deployments into the Labrador Sea as any remote operations in this harsh environment require significant effort and skill in post-processing the data. Chapter 3, reviews the collected data, the strategy and methods with which we processed data. Chapter 4, discusses the glider sensor data with regard to the earlier raised questions on improving CO_2 sensing capability, while Chapter 5 explains glider oceanographic and other observations in the Labrador Sea not discussed explicitly in Chapter 4. The final section - Chapter 6, summarizes results of this work with an outlook for carbon sampling in this region using gliders and other autonomous platforms.

Chapter 2

Background

2.1 Labrador Sea

The oceanography of the Labrador Sea is complex and fascinating. The strong seasonal character of high latitude oceans is present on all scales with strong gyres fed by the Atlantic and polar glaciers from the Arctic that give rise to strong gradients in temperature, salinity, eddies, jets and turbulent mixing plumes (Clarke and Gascard, 1983). Severe storms, harsh temperatures, sea ice – makes this place a real ocean frontier. Yet, this harsh environment is full of life, and this abundance, in physical and biological terms, has created a unique ecosystem. Being a gateway to the Arctic adds another strategic and political layer to the Labrador Sea and its bordering countries. The literature on this region is voluminous, here we briefly review some of the geography and oceanography of the Labrador Sea (Lazier and Wright, 1993; Cuny et al., 2002) with a focus on the winter period deep vertical convective mixing (Lazier, 1973; Clarke and Gascard, 1983; Lilly et al., 1999). We focus our review on

the importance of this region for global marine CO_2 sequestration and transport as part of ongoing research efforts on carbon uptake by the ocean (Sabine et al., 2004; DeGrandpre et al., 2006). Over the past twenty years, there have been several masters and doctoral theses on this region that have greatly benefitted the content of this Chapter (Frajka-Williams, 2009; Landschützer, 2014; Wolf, 2017).

2.1.1 Geography

The Labrador Sea is located in a deep, roughly oval-shaped basin (on average about 3500 m deep) in the Northern Hemisphere between the coastlines of Labrador and Greenland to the West and East, separated in the North by a shallower sill (approximately 1000 m deep) from Baffin Bay; and meets with the North Atlantic to the South. The Labrador Shelf is shallow (less than 500 m) and much more extensive (over 200 NM) than the shelf on the Greenland side, just 10-20 NM to the shelf break. Sharp topography on the Greenland and Labrador Side constricts Arctic airflow giving rise to the substantial fall and winter Northeasterly winds feared by seafarers.

Proximity to the Arctic results in active biological seasonal cycles where the injection of nutrients caused by upwelling from glaciers and ensuing transport from currents cause intense blooms of phytoplankton in the spring (Arrigo et al., 2017). Increasing sea ice decline in the Arctic as part of climate change are extending bloom conditions and second blooms in the fall have been observed (Ardyna et al., 2014). The cold winds and temperatures also lead to significant sea ice presence on the shallow Labrador Shelf side in most of the years, but ice is not as extensive on the Greenland side (Parkinson, 2000). Sea-ice cover extends over the majority of the
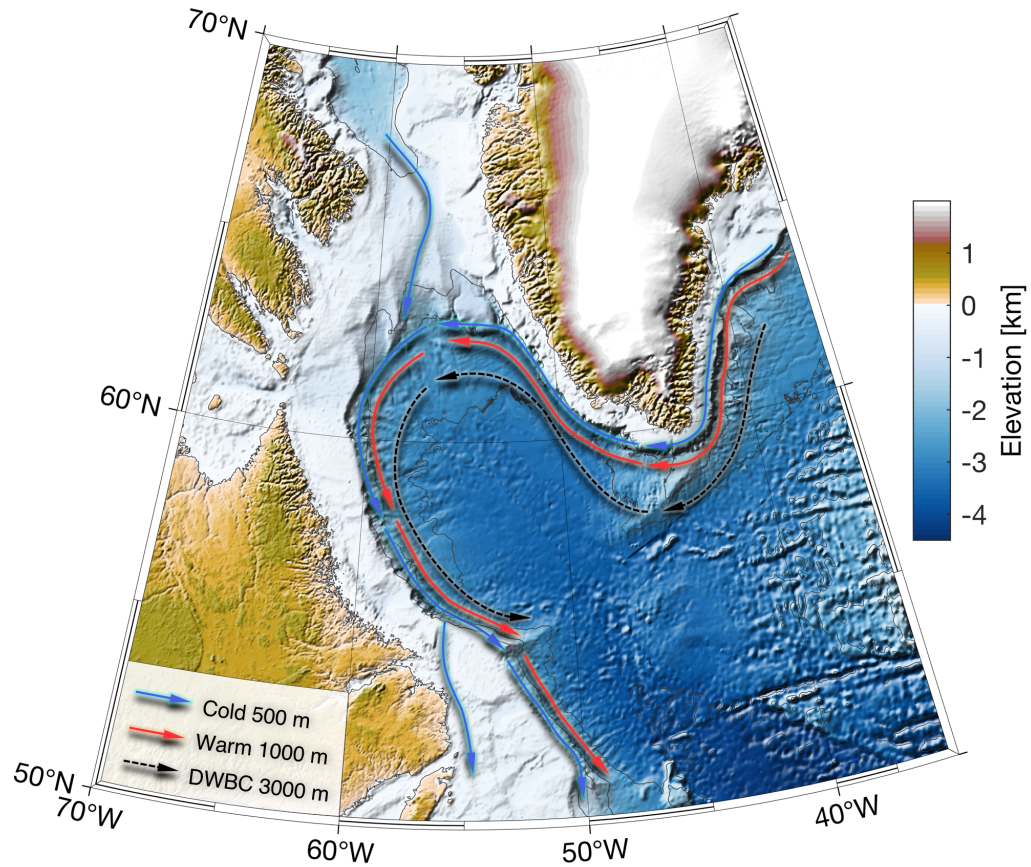
Figure 2.1: Map for the Labrador Sea Region. Arrows indicate the approximate path of the cyclonic gyre circulation, including the Deep Western Boundary Current (DWBC). Colors indicate major topographic features.

Labrador shelf, forming in mid-Winter and usually staying until mid-May to early June before being swept South, although formation is not zonally uniform and there is considerable interannual variability in sea ice cover (Prinsenberg et al., 1997). In pack ice formations, strong ice pressure ridges can form keels up to 20 m deep (Sudom et al., 2011) in some places extending to the seafloor, anchoring drift ice, resisting

winds and currents. Sea-ice is also an important region for the local population in terms of mobility for fishing, and hunting and travel as many coastal communities are without roads (Bell et al., 2014). Winds cause shear and cracks in the ice that form open water zones or Polynyas, and these tend to repeat in the same location making them essential to local marine life and the people that depend on them (Stirling, 1980; Schledermann, 1980; Durkalec et al., 2015). Greenland's glaciers inject many icebergs into the Labrador Sea, travelling southwards along the Labrador Coast until meeting the warmer North Atlantic near Newfoundland, making this region colloquially known as iceberg alley (Robe et al., 1980). These white bolides are a silent reminder of the Arctics enduring influence on the North Atlantic.

2.1.2 Circulation

The main circulation pattern in the Labrador Sea is cyclonic, consisting of the West-Greenland Current (WGC) on the western part of the basin and Labrador Current (LC) to the east. These shallow and narrow jets flow along the coastal shelf breaks slopes, with mean WGC transports of 3 Sv ($1 \text{ Sv} = 1 \times 10^6 \text{ m}^3 \cdot \text{s}^{-1}$) measured at Cape Farewell (Clarke, 1984) and LC summertime transport of 11 Sv, but seasonal variations of up to 4 Sv noted by Lazier and Wright (1993). The changes in flow strength are influenced by Arctic freshwater flux (Lazier and Wright, 1993). This gyre rotates waters along the Greenland and Labrador coastlines leading to almost saucer-shaped isopycnals in the basin (Lazier, 1973). The WGC introduces warmer-salty water from the Irminger Sea (ISW) and cold-fresh water from the Nordic Seas to the Labrador Sea. This duality results in a layered flow with fresh-cold ($\theta \approx -1.8°\text{C}$

and S ≈ 34.4 PSU) water at the surface and ($\theta \approx 4.5°$C and S ≈ 34.9 PSU) ISW at the bottom of the flow (Cuny et al., 2002). The Labrador Current is fed by Baffin Bay, glacial waters, cold-fresh and nutrient-rich, with ($\theta \approx -1.5°$C and S ≥ 34 PSU). ISW has been observed to travel around the basin below this fresh part of the LC preserving the layered structure of the WGC (Cuny et al., 2002). This cold and nutrient-rich water feeds the fertile spawning grounds that makes Newfoundland and the shores of Labrador important fishing grounds for codfish and salmon, both of which have substantially declined in recent decades (Brice-Bennett, 1992; Murray et al., 2007). The deep circulation in this basin is cyclonic consisting of the Deep Western Boundary Current (DWBC) flowing along the 3000 m isobar, carrying North Atlantic Deep Water (NADW) and denser Denmark Strait Overflow Water (DSOW) south. Both currents systems flow into the North Atlantic passing by the Flemish Cap Fischer et al. (2004). Figure 2.1 shows the topography (elevation and bathymetry) of the region, with Labrador (LC) and West Greenland Currents (WGC) divided into fresher (blue) and saltier (red) layers, coinciding with 500 and 1000 m isobaths. Dashed arrows indicate the approximate path of the Deep Western Boundary Current (DWBC) along the 3000 m isobath.

The basin gyre circulation follows the contours of f/h, where f is the Coriolis parameter and h is bathymetry (Cuny et al., 2002). Changes in bottom topography and conservation of potential vorticity lead to frontal instability that gives rise to buoyant anti-cyclonic eddies on the Greenland and Labrador shelf that propagate inward observed from satellites and gliders (Hátún et al., 2007). A particular type of eddy sheds off Cape Desolation (Greenland). These are called Irminger Rings (Lilly et al., 2003). Another source of eddies is the baroclinic instability observed in the

central basin influenced by the layered gyre structure. Under the influence of winds or propagation of other activities, the weak stratification gives rise to small scale jets and vortices can mix water vertically to depths over 1000 m and play important roles in restratification of the Labrador Sea after wintertime mixing (Lilly and Rhines, 2002). These interior eddies are believed to regulate heat loss and restratification of the water following wintertime mixed layer erosion (Katsman et al., 2004). Chanut et al. (2008) categorizes these eddies based on the instability source and general region in which they occur.

2.1.3 Convection

The Labrador Sea is one of few ocean regions, where wintertime mixing of the surface layer can reach depths of up to 2000 m (Lazier, 1973; Marshall and Schott, 1999). This deep convection forms a characteristic water lens that occupies a large volume of the Labrador Sea, termed Labrador Sea Water (LSW). The LSW occupies a large volume inside the basin from about 500 to 2000 m in depth and is observed in most of the intermediate depths (1000 to 3000 m) of the North Atlantic and along the Western Boundary past the Equator (Wallace and Lazier, 1988). A Temperature–Salinity (T–S) signature uniquely identifies this water mass from the time that it formed that varies between convection years.

The exact process by which deep convection occurs in the Labrador Sea has been studied for decades and researchers mostly agree on a basic three-phase model adapted from the Mediterranean Sea by Lazier (1973) and Clarke and Gascard (1983). In this model, the process begins with the conditioning of the interior region by the cyclonic

12

boundary currents. The horizontal slope of the isopycnal contours draws weakly stratified boundary current water to the interior region. Cold Arctic winds drive surface layer heat loss of over 1000 W/m^2 (Lilly et al., 1999) that further erode the stratification of the surface mixed layer. The second phase starts with storm events or other sources of energy such as eddies, that perturb the delicate vertical balance causing the water column to collapse in the form of turbulent mixing jets or plumes. These plumes quickly mix downward, reaching sometimes up to 2000 m deep (Clarke and Gascard, 1983; Lilly et al., 1999). The resulting mixing exchanges energy in the form of heat and, following a very energetic and short-lived convection period, the surface re-stratifies. This is also referred to as ventilation (van Aken et al., 2011). This intense mixing is made possible by a weak salinity gradient in the Labrador Sea between the surface and the intermediate-depth (200 to 1000 m) water. Finally, spring sea ice melt and warming temperatures restore the density stratification in the water column, forming a several hundred-meter thick surface layer on top of the newly formed LSW, visible in hydrographic sections with its distinct density signature. The final stage of the LSW formation process is the spreading of the water mass along isopycnal slopes of deeper bottom water, feeding the lower limb of the Meridional Overturning Circulation (MOC), pushing this nutrient-rich and oxygenated water mass to greater depths as it travels south along various pathways (Lumpkin and Speer, 2003). Improved knowledge surrounding the LSW formation process is crucial to improving our understanding of the thermohaline circulation model (Broecker, 1991) and the Labrador Sea an important ocean site to understanding the implications of climate change (Kieke et al., 2007). The circulation and transport of LSW is not a significant focus of this background section, but drifter work by Van Sebille et al.

(2011) focused on DWBC transports have shown latency between LSW formation and travel to 26°N of approximately 4 years.

Significant inter-annual variability exists in both the strength of convection and volume of LSW production. Pickart et al. (2002) explain this variance through correlation with the dominant mode of atmospheric variability called the North Atlantic Oscillation (NAO). However, in more recent years this explanation has been deemed too simplistic by the general oceanographic community (Chanut et al., 2008). Yashayaev (2007) has shown this variability in LSW formation extends to decadal and multi-decadal cycles, including years with no convection, from over 40 years of hydrographic data. Earlier observational studies in the 1960s (Clarke and Gascard, 1983), describe years with no convection at all, coinciding with a period of low salinity anomalies between 1968 – 1982 (Dickson et al., 1988). This distinct period called the Great Salinity Anomaly of the North-Atlantic is thought to be the result of increased polar freshwater influx advected through the North Atlantic current system and thereby changing convection and LSW formation (Malmberg, 1969; Lazier, 1980). Work by Broecker et al. (1985) and Aagaard and Carmack (1989) pointed towards the danger of increased melt rates in the Arctic and shutdown of convection driven overturning circulation. Most recently Lozier et al. (2019) summarized the work of the Overturning in the Subpolar North Program (OSNAP) – a multi-national effort to directly measure the overturning circulation that forms in the North Atlantic. Based on the OSNAP data, Lozier et al. (2019) challenge the prevailing view of the role of LSW formation and MOC strength (Broecker, 1991). Their data (collection started summer 2014) points towards the Irminger and Iceland basins as hot spots for explaining the variability in the MOC strength of the subpolar gyre and a weaker signature of the

14

Labrador Sea towards the overturning circulation across the Subpolar North Atlantic, but note the importance of freshwater flux on total transport budgets. The authors of the study, however, acknowledge that more data is needed to capture variability that could exist on longer time scales. The Labrador Sea convection is still a vital heat sink for the world ocean warranting a continued focus on convection strength and variability in LSW formation.

2.1.4 Labrador Sea and the CO_2 Sink

Increasing greenhouse gas concentrations, such as CO_2 from burning fossil fuels have far-reaching influences on our climate. According to the latest report by the Intergovernmental Panel on Climate Change (IPPC), the increased atmospheric CO_2 concentrations have already caused an increase in global temperatures by $1.5°C$. The increasing trend of atmospheric CO_2 levels is also being detected in our oceans with far-reaching consequences to marine life. In fact, we now know that the ocean is responsible for the yearly uptake of about 26% of anthropogenic CO_2 emitted into the atmosphere (Le Quéré et al., 2015). Through this uptake, so far the world's oceans have had a moderating effect on the progression of global anthropogenic climate change taking up roughly one-third of all anthropogenic carbon emissions since the start of the industrial revolution (Khatiwala et al., 2013). Sabine et al. (2004) compiled available marine CO_2 measurements and showed a strong latitudinal increase of anthropogenic CO_2 content in the North Atlantic, with highest concentrations found in the subpolar regions such as the Labrador Sea. Researchers such as Takahashi et al. (2002) on the other hand compiled atmospheric and marine surface measurements of

pCO$_2$ and used the methods from Wanninkhof (1992) to compute atmospheric flux rates for the global ocean as well as looking at seasonal variations due to effects of biology and temperature. His results similarly showed the most considerable flux to occur in subpolar regions such as the Labrador Sea, although his results also showed a substantial seasonal variability from biogenic factors. Watson et al. (2009) also showed that the North-Atlantic is one of the most active sinks of anthropogenic CO$_2$ in the Ocean. Earlier tracer experiments by Wallace and Lazier (1988) similarly pointed to the Labrador Sea convection region as a critical driver in air-sea exchange and uptake of atmospheric gasses.

Theory suggests that atmospheric interaction from storms coupled with high solubility gradients strengthen air-sea fluxes in the North Atlantic, together with deep drawdown through deep wintertime mixing (Clarke and Coote, 1988; DeGrandpre et al., 2006; Körtzinger et al., 2008). This has led to notions of the Labrador Sea as a sink for atmospheric carbon. This points to the importance of the Labrador Sea for CO$_2$ uptake and the relevance of programs such as VITALS. Current estimates put Atlantic Ocean anthropogenic CO$_2$ uptake to $-0.45 \pm 0.15\,\mathrm{PgC \cdot yr^{-1}}$ (Landschützer et al., 2014). However, questions remain as to how much of this contribution is due to the Labrador Sea alone. Much uncertainty remains around how the CO$_2$ uptake in the Labrador Sea is expected to respond to future global warming and salinity changes due to polar meltwater entrainment (Dickson et al., 2007). This might have severe impacts for global atmospheric CO$_2$ levels further exacerbating greenhouse effects with implications on marine and terrestrial ecosystems on all scales (Stouffer et al., 2006).

2.1.5 Wind-Driven Air-Sea CO_2 Flux Models

The previous section pointed to the Labrador Sea as a global sink for atmospheric CO_2. Here we discuss conventional methods to quantify the exchange of CO_2 between ocean surface water and the atmosphere and their relevance to estimating CO_2 uptake in the Labrador Sea. The relationship between atmospheric CO_2 (xCO_2) and oceanic uptake is usually expressed in the form of bulk flux calculations, were k is the gas transfer velocity (typically mol·s^{-1}) and pCO_{2w} and pCO_{2a} refer to the partial pressure of CO_2 at the bottom (surface) and top (air) of the sea surface boundary layer across which the flux is to be estimated. This approach is based on a simple model in which mass transport is constrained by turbulence and molecular diffusion (Jähne et al., 1987; Landschützer, 2014). The ocean in such a model is either taking up or outgassing CO_2 and was the basis of the uptake maps produced by Takahashi et al. (2002). This model is somewhat simplistic as it is centred on the surface mixed layer of the ocean. Multi-layer approaches have also been developed, such as Sarmiento (2006), where gas transport is governed by Fick's first law. For the Labrador Sea wintertime convection, however, where mixed layer depth occasionally reaches to depths over 2000 m, this approach can be used to represent the deep ocean sequestration of CO_2.

$$\frac{d[CO_2]}{dt} = k(pCO_{2w} - pCO_{2a}) \tag{2.1}$$

In the above formulation, the transfer velocity k is the primary factor that connects air-sea gas exchange to the state of the atmosphere. Jähne et al. (1987) was the first to propose a relationship between wind speed (although he called it friction velocity) and Schmidt number (Sc). Wanninkhof (1992) proposed an empirical method

to compute the Schmidt number for CO_2 for temperatures between 0 to 30°C and salinities between 0 to 35 ppt. Wanninkhof, using wind tunnel studies, came up with a quadratic relationship of the wind speed at 10 meters (U_{10}) compared with Jähne's friction velocity. However, different parameterizations of this wind speed coefficient have since been published (Nightingale et al., 2000), and Wanninkhof himself later revised his wind speed relationship to cubic (Wanninkhof and McGillis, 1999).

The above models and parametrizations are only an approximation for the total net flux of CO_2 between the atmosphere and the surface ocean. As stated in the paragraph above, due to the deep mixing in the Labrador Sea in the winter and early spring, surface CO_2 concentrations occasionally mix to depths greater than 2000 m. This makes a 2-layer bulk model a possible approach to estimate total uptake in this particular region. The above models require measurements of the oceanic and atmospheric partial pressure of CO_2. The next section will describe the implication of increased CO_2 uptake into the Labrador Sea, highlighting the need for continuous monitoring of marine carbon parameters. The remainder of the chapter will describe ocean gliders as a measurement platform for the Labrador Sea and introduce various mobile in-situ CO_2 sensor technologies with a focus on measurable marine carbon parameters.

2.2 Implications of Labrador Sea CO_2 Uptake

During the Labrador Sea deep convection phase, atmospheric CO_2 enters the deep ocean and is distributed globally through deep water mass transports. However, increasing CO_2 concentrations and marine life exist in a delicate balance. The carbonate

equilibrium reactions (Millero, 2007), show that in presence of seawater, CO_2 undergoes spontaneous dissociation to carbonic acid, releasing free hydrogen ions (Equation 2.2a and 2.2b). These free hydrogen ions (H^+) are neutralized by carbonate (CO_3^{2-}) ions in water (Equation 2.2c), released from calcium carbonate minerals (Equation 2.2d).

$$CO_2(g) \rightleftharpoons CO_2(aq) \tag{2.2a}$$

$$CO_2(aq) + H_2O \rightleftharpoons H^+ + HCO_3^- \tag{2.2b}$$

$$HCO_3^- \rightleftharpoons H^+ + CO_3^{2-} \tag{2.2c}$$

$$Ca^{2+} + CO_3^{2-} \rightleftharpoons CaCO_3(s) \tag{2.2d}$$
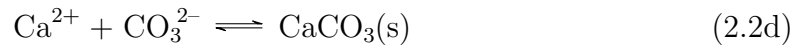
Increased CO_2 concentrations in an marine environment can completely deplete available carbonate ions to the point where H^+ and HCO_3^- ions begin to dissolve calcium carbonate minerals ($CaCO_3$) found in most marine organisms, disrupting ocean life. The decrease in pH levels from increased H^+ concentrations is termed Ocean Acidification (OA). This phenomenon has brought under threat entire ecosystem such as the Great Barrier Reef in Australia (Cohen and Holcomb, 2009). The potential for calcium carbonate mineral to undergo dissolution into carbonate ions due to carbonic acid is defined by its saturation state (Ω) and is controlled by the product of dissolved carbonate mineral ion concentrations and its equilibrium constant (K_{sp}).

$$\Omega = \frac{[Ca^{2+}][CO_3^{2-}]}{K_{sp}} \tag{2.3}$$

If $\Omega \geq 1$ then calcium carbonate dissolution does not occur. If it is less, then calcium carbonate mineral will dissolve in seawater, including calcium carbonate from shells found in most of marine life. The most common naturally occurring forms of calcium

19

carbonate mineral in seawater are calcite and aragonite and it is common to express calcium carbonate saturation states for aragonite and calcite. The abundance of carbonate ions in a given body of water, with a particular temperature, salinity will lead to depths where saturation drops below equilibrium required to maintain mineral $CaCO_3$. This saturation depth forms a chemical boundary whereby water becomes to corrosive for marine life to calcify and survive.

Researchers at the Bedford Institute of Oceanography (BIO) are studying how the saturation horizon for calcite and aragonite are affected in the Northwest Atlantic. From ship cruises and bottle samples, in 2010, the estimated Labrador Sea calcite saturation depth reached to 2300 m, coinciding with the LSW formation depth. Aragonite saturation depth similarly fell within water mass boundaries between LSW and NEADW (Azetsu-Scott et al., 2010). As CO_2 concentrations continue to increase in the atmosphere, these saturation ceilings could change rapidly with deep convection in the Labrador Sea. The formation of a large volume of LSW with high dissolved CO_2 concentrations could rapidly deplete available carbonate ions, decreasing carbonate mineral saturation horizons. Such a scenario would threaten the entire Labrador Sea ecosystem. Not to mention the Labrador Sea is home to deep water corals, whose ancient lives may hold untapped clues to the fragile balance of life in the past (Adkins et al., 1998; Sherwood and Edinger, 2009). Due to the links between the Labrador Sea water formation and the global ocean, such rapid changes to the seawater chemistry in the Labrador Sea would have strong implications for marine life elsewhere. Acidic LSW would eventually make its way to other parts of the ocean, disrupting marine life in those habitats. As climate change continues to affect physical cycles in the ocean and ecosystem health, accurate knowledge of carbonate ion concentrations,

pH levels and pCO_2 will continue to matter to nations and stakeholders around the world.

2.3   Measurable Marine CO_2 Parameters

CO_2 in the ocean, despite its importance to crucial climate processes, is still poorly sampled. Long term (monthly sampled) time series (since 1980) only exist in a few places, e.g. the Hawaii Ocean Time Series (HOT) and the Bermuda Atlantic Time Series (BATS) and mostly rely on ship support (Dore et al., 2009; Ducklow et al., 2009). The ocean is still severely undersampled with respect to chemical observations. The cost of ship-based observations and increasing funding challenges to large scale observing programs, has led some researchers to call for an autonomous biogeochemical observing network (Johnson et al., 2009) to increase the resolution of observations. However, this observing component development requires stable measurement techniques from in-situ platforms, a challenge that is not yet overcome. Improvements in resolution and frequency of surface CO_2 measurements have been made with the development of stable ship-based in-situ measurement systems installed on vessels of opportunity (VO) such as containerships or tankers with regular routes across ocean basins. These results made possible the creation of a $1°$ global resolution (up to $1/4°$ coastal zones) Surface Ocean CO_2 Atlas (SOCAT), initially released in 2011 and currently distributing the 6th version of this product (Bakker et al., 2016). Any of two of the measurable carbon parameters: pH, Total Alkalinity (TA), the partial pressure of CO_2 (pCO_2) and Total Inorganic Carbon (TIC) are sufficient to calculate all remaining carbonate system variables in relation to each other. These variables are

used to compute other carbon parameters such as DIC (Dissolved Inorganic Carbon) through equations (Lewis et al., 1998). Of all measured CO_2 parameters, pCO_2 is probably the most prolific measured parameter today due to its relationship between atmospheric concentration and CO_2 flux into the surface ocean through bulk flux calculation methods discussed previously.

Traditional measurements of pH, TIC, TA and pCO_2 are typically done through discrete sampling from shipboard CTD-rosettes equipped with Niskin bottles. Bottle samples are taken and analyzed on board the vessel or later on shore using infrared, electrochemical, spectrophotometric (Clayton and Byrne, 1993) and mass-spectrometer type (Yao and Byrne, 1998) methods to analyze gas content and elemental composition of CO_2 in seawater. A great deal of effort is expended in proper sample preparation and avoiding contamination from biogenic and atmospheric factors after the sample is taken. Correct salinity and temperature information are also required. On the other hand, in-situ methods are still not very common except for pCO_2 and pH (Clarke et al., 2017a). These components have been reliably measured through infrared (IR) detection in equilibrator type (DeGrandpre et al., 1995) and glass-electrode approaches (Dickson, 1993). There is a strong push in the biogeochemical community to increase and expand available in-situ technology to other carbon variables and decrease dependence on ship cruises. Also measuring carbon parameters in a discrete sampling way makes it difficult to resolve some of the very localized and short time scale processes by which carbon enters the coastal and open ocean important for getting the physics right in biogeochemical models (Denman and Gargett, 1983; Sarmiento and Gruber, 2002). The next sections will discuss the current state of CO_2 in-situ sensor technology with a particular focus on mobile platforms

such as gliders and floats.

2.4   Gliders used for Labrador Sea Observing

Gliders are small cylindrical shaped ocean observing platforms that use changes in buoyancy to float up and down and generate lift by its wings to achieve forward motion. This makes gliders very energy efficient and missions of up to a year are possible (Eriksen et al., 2001). Missions of 4 to 6 month are routine. Upon surfacing, gliders relay information via satellite to the shore servers, offering a close to a real-time look at ocean environments. Typically, gliders are designed for diving to 200 or 1000 m in depth, although new gliders are being tested to go as deep as 6000 m (Osse and Eriksen, 2007). Seen as a visionary solution to achieving higher spatial and temporal ocean resolution to fill gaps left by other observing platforms (Stommel et al., 1989), hundreds of gliders today are used on all continents and ocean regions and collecting valuable high-resolution data for the ocean science community. In conjunction with its sibling instruments, Argo floats of the International Argo program; gliders have become a central part of the Global Ocean Observing Systems (GOOS) (Testor et al., 2010, 2019).

Gathering data through gliders offers several advantages, compared to traditional ship-based surveys, because they are cheaper and easily adaptable to different missions. Autonomous platforms also require less personnel and data can often be accessed in near real time making them ideal for ocean monitoring applications. Called autonomous, though mostly operated by human-pilots through computer commands and scripts, these vehicles are not as self-reliant as their name might suggest. Adaptive

sampling and path planning work is being done to take away some of the significant efforts on the part of the pilot to keep these vehicles alive during long deployments (Fiorelli et al., 2003; Alvarez and Mourre, 2012). On the downside, they move more slowly (1 km/hr) than ships, meaning time variability is easily aliased as spatial variability (Rudnick, 2016). This makes gliders only moderately suitable for basin-scale observing and most work with gliders has focused on the coastal and intermediate zones, studying shorter spatial scales (Rudnick, 2016). More importantly, glider platforms impose a range of restrictions on the type of sensors a glider can carry. Sensors must be small in size to avoid negative impact on hydrodynamic efficiency and must be low weight not to shift the centre of gravity, negatively affecting the buoyancy of the system. The most stringent restriction gliders place on potential sensor probes are restrictions on power consumption that dictate the battery budget and viable length of a mission (Rudnick et al., 2004). Sensors need to be designed explicitly for gliders, and already available sensors that work well with other platforms may not be at all suitable for gliders without substantial modification and testing.

Doing glider work in any remote regions has many challenges, especially in the Labrador Sea. The distance from nearby coastal communities typically requires a ship for launch and recovery or significant battery budget constraints to operate for long periods remotely, constraining the scientific mission. Launching from a ship has certain advantages, as it allows concentrating battery power on collecting relevant scientific data, but increases the cost of the mission, environmental footprint and limits deployment to the ship's availability. Launching from shore brings independence, but requires skill in piloting and can take away months from the mission. Such a launch into the Labrador Sea is a little easier to do from Greenland than Labrador shelf

side because the shelf break is closer to the coast and gliders can dive to their full depth sooner, making the buoyancy pump more efficient. Launching on the Labrador side would require a glider to dive to 100–200 m for 200 NM, while also confronting the strong boundary currents. As most of the battery draw on a glider comes from the buoyancy pump, increasing dive cycles would result in higher energy loss over a shorter distance.

To date, there have been about a dozen glider missions with sampling focus on the Labrador Sea. Of these deployments, notably Howatt et al. (2018) used a Labrador shelf glider deployment with repeat shelf crossings to quantify heat and salt transports. Frajka-Williams et al. (2009) looked at meso- and sub-meso-scale links between physical water properties and the phytoplankton blooming, comparing glider and satellite measurements. Eriksen and Rhines (2008) deployed sea gliders from Baffin Bay over several years between 2003–2005 with recovery in Nuuk to collect hydrographic data of the deep convection zone. Several crossings of the deep convection zone during the winter time were analyzed in Frajka-Williams et al. (2014) to study the restratification process following deep convection.

Recently, the first glider mission into the central Labrador Sea without the use of a ship for launch and recovery from the Labrador Shelf was by deYoung et al. (2018). The glider was deployed in Cartwright (coastal Labrador) and then crossed the shelf current using a thruster, reaching the study area after a month. The thruster cost significant battery power but was necessary to limit southward advection in the shelf current. This deployment strategy allowed for about two months of continuous sampling in the deep convection area of the Labrador Sea from 3 October to 22 November 2016. Upon return to Newfoundland, the glider had less than 20% of

overall battery power remaining. This was a pioneering mission in the sense that the glider completed the entire track without assistance from a ship.

2.5   Mobile in-situ CO_2 Sensors

The selection of mobile in-situ CO_2 sensors that are available to research groups is limited. Manufacturers such as Aanderaa Data Instruments (ADI) and SeaBird Scientific are developing CO_2 and pH sensors that have undergone limited field testing through select scientific groups. However, the only CO_2 system variables routinely measured on remote platforms today are pH and pCO_2 (Clarke et al., 2017b). Other new approaches are using micro-fluidic chip sensors to measure alkalinity at the National Oceanography Centre (NOC) based on previous successful work to create a nitrate sensor (Beaton et al., 2017). Yet none of the available systems has been designed specifically for ocean gliders. Notably, the current selection of pCO_2 probes is foil based photo-chemical (optodes) and non-dispersive infrared refraction (NDIR) gas analyzers (colourimetry). Recently the Wendy Schmidt Ocean Health X-PRIZE competition (Okazaki et al., 2017) resulted in a new class of pH sensors based on the Ion-Sensitive Field-Effect Transistor (ISFET) technology. These sensors have been adapted and marketed by SeaBird for use on autonomous floats (APEX float), but not yet commercially available for gliders. Recent work by Saba et al. (2018), in cooperation with SeaBird, has beta tested a glider version of the sensor and has shown promising results.

For gliders, optical optode sensors are the only type of gas-sensor technology that can provide resolution and power consumption amenable with the operating

requirements of these platforms. For oxygen, this type of sensor is already widely used and well-characterized (Bittig et al., 2014). In Atamanchuk et al. (2014) a similar size CO_2 sensor was developed using Dual Lifetime Referencing technique (DLR) based on luminescent quenching. This type of sensor uses a special sensing foil that reacts to changes in pH in ambient seawater, detected as phase shifts in the emitted luminescent signal inside the sensor. In recent years, other groups, notably Clarke et al. (2017b) have developed similar sensors with improved foil chemistry that not yet made it to the commercial market stage. However, optical foil based pCO_2 sensor data output is entirely tuned by prior calibration data, and the foil chemistry suffers from instability when tuned towards high sensitivity (S. M. Borisov, *personal communications*) necessary in cold region deployments. The other prolific type of in-situ pCO_2 sensor is based on non-dispersive infrared refraction (NDIR) for example Pro-Oceanus CO_2-Pro CV^{TM} and CONTROS Hydro C^{TM}. This sensor type has significantly higher stability but is bulky, takes a long time to equilibrate and more power intense compared to optical probes, making neither system ideal. Here, we provide an overview of contemporary pCO_2 and pH sensing approaches suitable for autonomous platforms.

2.5.1 CO_2 Optode

The ADI, model 4979 CO_2 optode (Atamanchuk et al., 2014), is an example of the few suitable sensors available today for glider based CO_2 monitoring and the only one that has been commercially sold to researchers outside the initial developing group. The sensor, albeit still in early prototype stages, has been used in a handful of

27

mooring deployments (Atamanchuk et al., 2015; Peeters et al., 2016) with reasonable results and is virtually identical in size to the O_2 optode model 4831, one of the more common oxygen sensors offered on autonomous platforms today made by ADI. This provides for relative ease of integration to glider and float platforms. The sensor has excellent low power characteristics at 80 mW at 5 seconds and 7 mW at 1 min sampling frequency and can, therefore, be deployed on multi-month missions. The sensor is housed in a titanium cover with an internal processing board and has a built-in temperature thermistor rated to 600 or optionally 1200 dbar. Communication with the sensor is through RS-232 12-pin serial bus.

To reiterate, the optode foil is based on dual lifetime referencing (DLR) technique using two different fluorescent indicators (luminophores) embedded inside a gas permeable polymer membrane coated on a sensor spot glass window. The first indicator is sensitive to changes in pH and responds with a change in the intensity of blue light-induced fluorescence. Because fluorescence intensity is sensitive to factors such as light (e.g. sampling is in the euphotic zone), a second reference indicator dye is incorporated into the foil, not sensitive to pH with similar emission spectra, but much longer fluorescence lifetime compared to the pH-sensitive compound (Atamanchuk et al., 2014). When the sensing foil is excited by a pulsating blue light diode inside the optode, each indicator provides separate fluorescence signals. The two excitation responses have a phase lag (ϕ_{DLR}) used to determine CO_2 concentrations through a multi-point calibration model. The sensor foil was developed for Aanderaa, by Pre-Sens Precision Sensing Gmbh in Germany, similar to the well established O_2 optode models manufactured by ADI. The manufacturing quality of the sensor foil and calibration significantly influence the performance of the sensor, and great care must be

taken not to damage the physically and chemically sensitive foils.

For the CO_2 Optode, pCO_2 is related to phase shift and temperature through a multi-point calibration model (Atamanchuk et al., 2014), with an eighth-degree polynomial fit between sensor phase readings and temperature readings. The published method (ibid., 2014) requires 27 foil calibration coefficients $(C_{(0,0)} - C_{(8,3)})$ for successfully calibrating the sensor to a range of oceanic conditions. The phase readings are also multiplied in a 3-degree polynomial with temperature to relate these to the temperature dependent polynomial coefficients $(C_{t_0} - C_{t_8})$ for the fitted phase-temperature pCO_2 surface. Using the sensor phase angles (degrees), this yields the base 10 logarithms of pCO_2. All sensors, especially photo-chemical based, are known to exhibit drift due to a conditioning period, as the sensors equilibrate to ambient conditions. Atamanchuk et al. (2014) suggest correcting any change in calibration model, for example, due to foil response drift, through subtracting a single reference point $pCO_{2,\text{ref}}$.

$$log(pCO_2) = C_{t_0} + C_{t_1} \times \phi + ... + C_{t_8} \times \phi^8 - log(pCO_{2,\text{ref}}) \qquad (2.4)$$

We note that this fit model is arbitrary and other lower polynomial fits could be used, depending on how laboratory testing proceeds. Trying to fit the sensor to such a large number of inputs in temperature and molar CO_2 readings requires a long testing time. Therefore, a lower number of calibration points would be desirable.

An issue with all sensors and in particular photochemical sensors is the impact of temperature on response time and ultimately sensor performance. Optode response time is typically slow compared to the speed of the glider. Gliders travel vertically at a speed of roughly 0.1 m·s^{-1}. For a thermocline 5 m deep, with a temperature

29

gradient of 10°C this would equal a temperature change of $0.2°C \cdot s^{-1}$, which could be to fast for the sensor foil chemistry to respond. These repeat temperature gradient inversions are difficult to resolve for low-power, non-pumped optodes, due to their strong temperature dependence, leading to additive errors over time unless the sensor is given a chance to equilibrate (e.g. through hovering at depth) (Bittig et al., 2014). Therefore, optode data from a moving platform require correction either through prior knowledge of the sensor response to temperature changes or through recursive data filtering. Another issue with foil chemistry on moving sensors is the impact of the boundary layer that invariably forms on the sensors as it transitions through the water column. Such a boundary layer will impact the sensor readings compared to the true ambient concentrations. The performance on gliders has been well characterized for Aanderaa oxygen optodes. For example, Bittig et al. (2014) investigated the impact of the boundary layer thickness on the response time of the sensor. Methods for drift correction during long deployments on Apex floats have also been published (Bittig and Körtzinger, 2015). For the CO_2 optode, such information and characterization are lacking, requiring each user to come up with their strategy to account for all the potential data quality issues during any deployment.

2.5.2 NDIR Gas Analyzer

The Pro Oceanus CO_2-Pro CV is an example of a non-dispersive infrared refraction (NDIR) based gas detector able to detect concentrations of molar CO_2 to the accuracy of up to 1 ppm (parts per million) in air and water. The sensor has been developed for over a decade and has a patented system of chamber equilibration that collects

the gas pressure inside a special headspace and measures the absolute molar fraction (xCO_2) from the gas stream in ppm. The Pro CV offers an internal zero-reference measurement (ZM) to assess internal drift capability using Soda-Lime scrubbers to strip CO_2 from the gas stream and asses the internal drift of the infrared detector from zero CO_2 concentration. This capability is also present in the CONTROS Hydro C^{TM} and was used extensively in Fiedler et al. (2013) to quality control pCO_2 data from an autonomous float during post-deployment data processing. To compute the pressure of CO_2 the gas chamber pressure and molar concentrations are multiplied.

$$pCO_2 = xCO_2 \times P_{headspace} \tag{2.5}$$

Some instruments remove water vapour pressure and must be corrected for that, but the Pro CV already measures the wet gas stream, and therefore this correction is not necessary. It is recommended to use this type of sensor with a pump ensuring a constant supply stream of water into the sensing chamber of the instrument and shortening the time it takes for the sensor to equilibrate the internal and outside gas pressures.

The CO_2-Pro CV and Hydro C sensor has been assessed in numerous field studies and has known accuracy and stability (Jiang et al., 2014). This sensor, albeit accurate and reliable, has notable major drawbacks compared to the previously discussed optode sensor, limiting its portability on gliders. IR based colourimetry requires a lot more energy to detect IR wavelength absorption, compared to the optode lifetime signal detection. The sensor uses 4 W to operate (with a pump) and 9.5 W during the warm-up period, much too energy-demanding for a glider. Because of the gas stream equilibration, the sensor responds slowly to strong gradients in temperature and gas

pressure such as in profiling applications, requiring around 15 minutes with a pump to fully equilibrate to ambient xCO_2 conditions (Pro-Oceanus Systems Inc., 2018). For the Pro CV, in particular, some components of the sensor are fragile, and it is not known how well the sensor would function under constant profiling modes over months. Another issue with this sensor is the size (38 cm long with 10 cm diameter). The current sensors do not fit on gliders without some special adaption. In recent years Pro Oceanus manufactured a smaller version (28 cm and 5.1 cm diameter) of the CO_2-Pro CV with lower power consumption: $0.4 - 0.6$ W at 1 Hz rate without pump (Pro-Oceanus Systems Inc., 2019), but still much more power demanding than the optode for comparison: 0.01 W at 1 Hz sampling rate. This sensor was experimentally tested on a glider in the Chukchi Sea (Hauri et al., 2018) and revealed long equilibration times (>1 min) and difficulty of employing current membrane technology glider for rapid profiling. By no means was this sensor modular within current glider payload capacity, requiring substantial modification of the vehicle to accommodate the sensor and pump, impacting hydrodynamic efficiency. However, this type of sensor has started to see successful use in float based applications (Fiedler et al., 2013), and it is possible that in the near future this sensor will shrink even further in size. This could make this sensor relevant for glider applications, decreasing the equilibration time issue through the use of another reference instrument (e.g. pH or optode sensor) to approximate vertical CO_2 gradients. It would be sufficient to use the NDIR gas analyzer at select depths as calibration points and use the reference instrument to resolve depth profiles fully.

2.5.3 ISFET pH Sensor

Through the Wendy Schmidt Ocean Health X-PRIZE Competition, a new type of pH sensor was developed at Monterey Bay Aquarium Research Institute (MBARI) in collaboration with Honeywell, called the Deep-Sea ISFET pH Sensor. ISFET stands for Ion Sensitive Field Effect Transistor. This technology has been successfully used in collecting high accuracy data on profiling mooring in Monterey Bay (Johnson et al., 2016). This sensor was adapted for autonomous applications such as the APEX float by SeaBird Scientific called the Sea-Bird SeaFET^{TM}, retaining the basic design from MBARI (Martz et al., 2010). The ISFET pH sensor works by measuring two different pH signals (external and internal) using the Durafet (Honeywell) solid state chloride selective electrode and an internal near perfect Nernstian response (salinity insensitive) reference electrode that is only temperature dependent (Takeshita et al., 2014). These two indicators have shown high stability in real oceanic test conditions (Bresnahan et al., 2014). In the presence of information on temperature and salinity from a CTD, the external electrode provides better accuracy (Miller et al., 2018) and can be used to assess internal drift of the sensor as is done in the integrated SeaBird SeapHOX^{TM} CTD-DO-pH sensor package. The sensor has been available for purchase and integration to APEX floats by SeaBird. In total, about 200+ floats with this sensor have been deployed so far as part of the ongoing international ARGO programs such as Southern Ocean Carbon and Climate Observations and Modeling Program (SOCCOM) (Russell et al., 2014).

This sensor was recently tested on a glider as part of a study led by Dr Grace Saba between Rutgers University and SeaBird Scientific to monitor pH levels off

Atlantic City, NJ, USA. The sensor was integrated into the CTD of a 200 m Slocum Glider and over several weeks showed excellent characteristics under repeat 200 m profiling modes (Saba et al., 2018). During the study, the team focused on questions of sensor stability under repeat deployments, power consumption and issues around sensor calibration. The sensor output is a reference voltage that is converted into pH (total scale) using pressure, temperature and salinity information from the glider CTD using equations from Johnson et al. (2017). Using pH measurements, together with Total Alkalinity–Salinity (TA–S) relationships can be used to compute pCO_2 to an accuracy within $\pm$ 11 μatm (Y. Takeshita, *personal communications*).

Chapter 3

Data and Method

3.1 Collected Data

As part of the Ventilations, Interactions and Transports Across the Labrador Sea (VITALS) project in 2016, two separate ocean observing platforms were deployed into the Labrador Sea: an underwater glider (deYoung et al., 2018) and a moored vertical profiler the SeaCycler (Send et al., 2013). These platforms resolve fundamentally different scales and ocean processes, but the deployment was designed to link these data sets together to provide better data about the spatial (glider) and temporal (SeaCycler) dynamics. A key aspect of the joint deployment was to use the glider in combination with SeaCycler to do in-situ tests and quality checks with a novel CO_2 optode sensor. Questions about the optode performance following inspection of the data from the Labrador Sea mission, led to more detailed glider based CO_2 optode testing in Trinity Bay in 2018. Here we describe the two deployments, including instrument setup and calibration and required processing to achieve a consistent data

set for further analysis and discussion in Chapter 4 and Chapter 5. Figure 3.1 shows various observing activities including SeaCycler, AR7W Stations, Glider T–S profiles for the Labrador Sea and Trinity Bay deployments.

3.1.1 Labrador Sea Deployment

As part of the VITALS program, a moored vertical profiler the SeaCycler (Send et al., 2013) and a G2 Slocum glider were deployed into the central Labrador Sea near the longtime German deep convection mooring K1. The K1 mooring, located about 25 km West of former OWS BRAVO (Avsic et al., 2006), has been deployed biennially since 1994 to monitor activity in the central deep convection patch in the Labrador Sea (Lavender et al., 2002). The objective of VITALS was to characterize the spatial and temporal structure of oxygen and CO_2 in the deep convection zone. Other research activities also took place in conjunction with VITALS, including a hydrographic section AR7W maintained by the Bedford Institute of Oceanography (BIO) and Argo floats released with several profiles captured near the SeaCycler site and the glider deployment area. Many coordinated observing efforts came together, utilizing multiple complimentary efforts across different scientific programs, relying on both traditional and novel observation approaches.

The SeaCycler was deployed near 52.22°W and 56.82°N, 30 km away from German deep convection mooring K1 (52.66°W and 56.56°N) to improve the vertical and time characterization of O_2 and CO_2 uptake in this region. The SeaCycler operation and deployment techniques are in detail described in Send et al. (2013). Briefly, it is an underwater winch assembly, parked at 600 m depth with an instrument float that
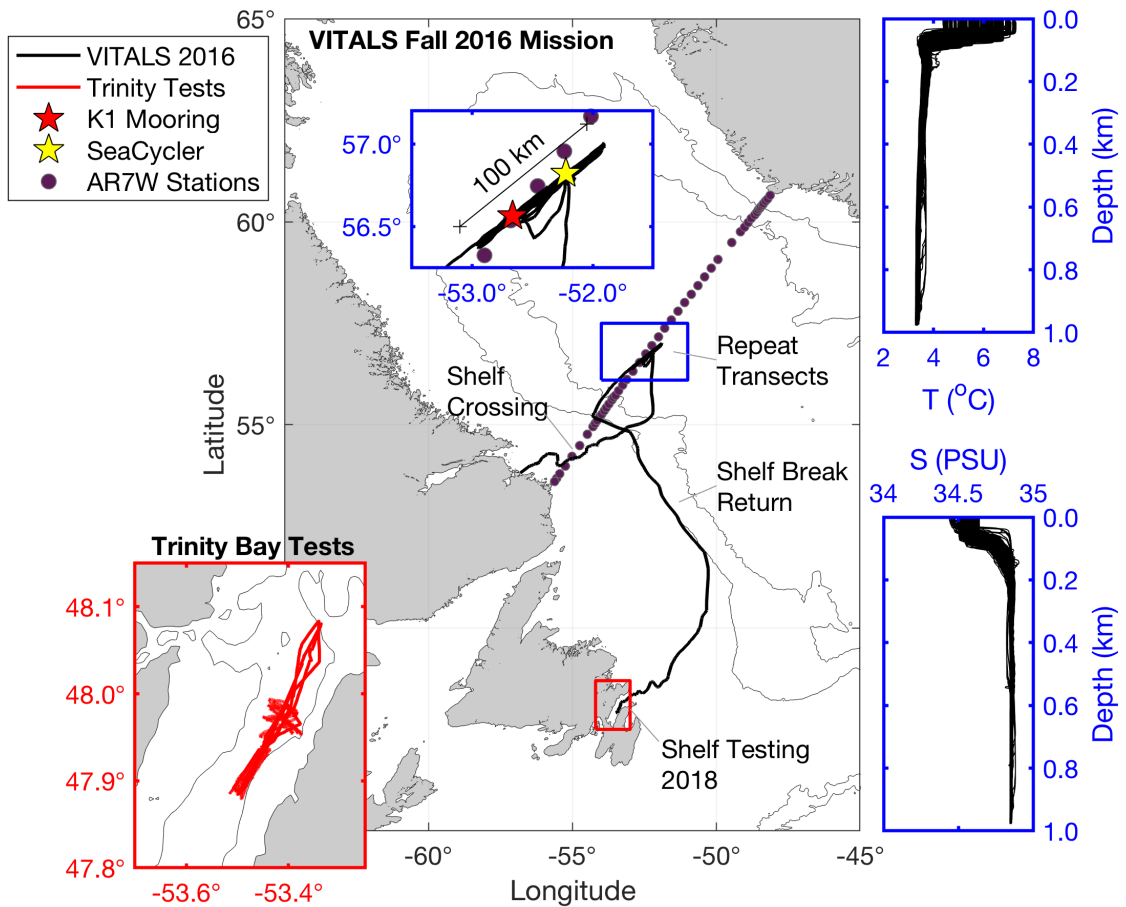
Figure 3.1: Map of data collection sites.

can profile the top 150 m. A tethered communication allows for two-way telemetry over Iridium Satellite. Below the winch assembly, a single-point mooring line with instruments continues to the ocean depth of approximately 3500 m. For this deployment, the instrument float carried CTD, ADCP and various gas sensors, including Clark-Type oxygen electrodes sensors (Seabird 41, Seabird 63), optodes (Aanderaa 4330 and CO_2 Prototype 4797), Nitrate (Satlantic Deep Suna), Fluorescence, Turbidity (Wetlabs) as well a bubble equilibrator infrared (IR) CO_2 gas analyzer Pro Oceanus CO_2-Pro CV, based on non-dispersive infrared refraction (NDIR) technol-

ogy made by Pro Oceanus Ltd of Bridgewater, NS (Canada). Previous tests with this sensor showed excellent stability in multi-month vessel-underway missions (Jiang et al., 2014). The instrument float collected data over the top 150 m of ocean depth with 0.3 m vertical resolution from June 2016 to May 2017, while the Pro CV was sampling for 20 minutes at select stop depths (10, 30, 60, 120 m) to allow equilibration with ambient seawater pCO_2. These stops resembled bottle stops done from ships to calibrate new sensors. The K1 mooring was also equipped with oxygen sensors to allow for later cross mooring comparisons.

In the Fall of 2016, a Slocum G2 (generation 2) glider (Unit 473) was deployed from the Labrador shelf to reach the K1 SeaCycler site and complete 30 to 100 km long transects between moorings, collecting high-resolution spatial data. The glider was launched near Cartwright, Labrador from a small fishing boat and reached the deep convection zone near K1 and SeaCycler early in October, sampling there until 22 November. In total, the glider completed 18 full transects collecting valuable hydrographic and gas data. The modified glider with an extended battery bay carried two optical gas sensors in addition to a SeaBird glider CTD: a novel Aanderaa Data Instruments (ADI) CO_2 optode prototype sensor (model 4797) described in Atamanchuk et al. (2014), reviewed in Chapter 2, and the well established Aanderaa oxygen Optode (model 4831, SN 333). The CO_2 optode (SN57) was equipped with a thicker slow response foil based on the recommendation we received (D. Atamanchuk, *personal communications*) to enhance long deployment stability. These sensors were mounted in the aft cone of the vehicle. Also, a thruster was installed to speed up the crossing of the shelf and to enable staircase profile sampling. The glider sampled the central Labrador Sea deployment location for two months, limiting CO_2 optode

38

profiles to the top 200 m to save energy. In December, the glider began its journey back to Newfoundland following the 1500 m isobath inside the Labrador Current and reaching Trinity Bay (see map) on December 31, 2016. The glider was flown along the shelf break to take advantage of the southward flowing Labrador Current. Before deployment on the glider, the O_2 and CO_2 optodes underwent rigorous testing at the biogeochemical laboratory facility at Dalhousie University to determine the calibration model fit for the optode sensor foils. Bottle samples were collected during the deployment of the glider to compute offsets for the glider's conductivity cell and any initial offsets for the glider optodes.

3.1.2 Trinity Bay Tests

After completion of the VITALS mission, not confident that the mission had tested all the characteristics of the new CO_2 sensor under glider profiling tests and in light of emerging requirements for ocean carbon observatories, we conducted further tests of the optode on a glider to learn more about the sensor. Trinity Bay, Newfoundland, a deep inlet (up to 600 m in the Eastern part), easily reached by boat from numerous coastal communities was chosen as a test site. It is fed primarily by the cold Labrador Current waters and river runoff from the western side making it's surface waters fresh and deeper portions frigid and highly oxygenated and nutrient-rich. The pooling of water in the deeper portion and surface freshwater produces a stable density stratification (Schillinger et al., 2000; Tittensor et al., 2002). Especially interesting for our optode tests are the large temperature gradients in the vertical of over 14°C between the surface and 75 m depth. Trinity Bay has a cold water lens -1°C between 70 m to

200 m depth, and temperatures below 1°C from 200 m to the bottom. In Trinity Bay profiling through this lens leads to absolute temperature gradients of 10°C or more, in 200 seconds or less.
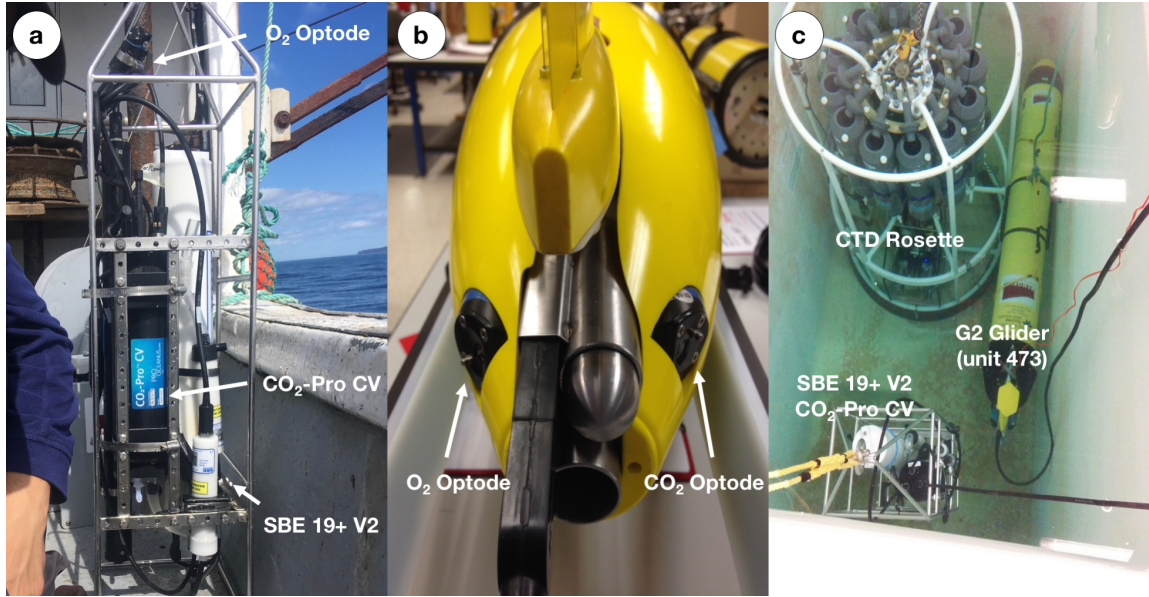
Figure 3.2: (a) Trinity Bay test reference CTD, (b) glider setup and (c) equipment tank testing in progress.

We re-deployed the glider with the same CO_2 optode sensor from the Labrador Sea mission, in Trinity Bay in September 2018 for 12 days. The glider sampled the same properties as in the Labrador Sea mission CO_2 optode sensor (SN57) with the same foil as well as another CO_2 Optode sensor (SN56). During the deployment, it was quickly realized that this sensor, which had the thinner fast response foil, was very unstable, and data was corrupted and was noisy. The encountered problems with the thin-foil are consistent with experiences by other research groups (S. Borisov and F. Peeters, *personal communications*). Therefore, we omit this data from the ensuing

chapters and discussions and focus instead on the sensor SN57 used in the VITALS deployment. We repeated step profiles as in VITALS and did extensive referencing of the sensor before the deployment and during using the same CO_2-Pro CV Sensor. Trinity Bay tests were mostly a repeated Labrador Sea mission on a smaller scale, except without the use of a SeaCycler. Instead, we used a winch operated Sea Bird Electronics (SBE) 19+ V2 CTD mounted on a frame, together with an O_2 Optode (Model 4831, SN 333) and a CO_2-Pro CV from Pro Oceanus. The setups for the external CTD and glider are summarized in Figures 3.2a and 3.2b.

We removed the extended bay and lithium battery pack and replaced it with an Alkaline battery pack that provided enough power for the deployment. We also removed the thruster added to the glider for the Labrador Sea mission. During the mission, it became evident that the onboard glider altimeter was not functioning correctly and we, therefore, constrained vertical profiles to 400 m depth. On a deep 1000 m glider the buoyancy pump is the most significant power draw (used twice every full dive cycle), and therefore the smaller depth profiles meant battery usage was not as efficient as one would have hoped. Due to the low temperatures and low depths, the new alkaline pack was nearly depleted by the end of the 12-day deployment (11.5 V).

Pre-deployment tests in laboratory tanks of the sensor and the glider allowed for rigorous instrument data quality control in this mission. We extensively calibrated the CO_2 and O_2 optode sensors using a double walled test tank, called a reactor with simultaneous O_2 and CO_2 supply for rapid step changes in these variables. We recorded the optode response in the range of $-1.8°C$ to $20°C$ and O_2 concentrations ranging from 0 to 120% saturation and CO_2 concentrations from 100 to 3000 μatm.

Tests were initially done in freshwater and repeated for 35 ppt NaCl solution. Total calibration of the CO_2 optode required several weeks. From this tank calibration exercise, new fits for the O_2 and CO_2 foils were recorded inside the sensor. Furthermore, tests of all sensors together were done at the special saltwater tank at the Department of Fisheries and Oceans (DFO) in St. John's, Canada. The tank facility is large enough to allow submerging the glider, CTD-Pro CV setup and a reference CTD rosette from DFO with high precision CTD, O_2, pH and Niskin bottles to collect reference samples for the instruments. From these measurements and tank calibration exercises, we computed instrument specific offsets used for later correction of the data during post-processing to achieve a coherent data sample. Instrument-specific offsets are provided in Appendix A. A picture of tank testing in progress is shown in Figure 3.2c.

3.2 Other Sources of Data

For the period of the Labrador Sea deployment, we obtained hourly atmospheric CO_2 concentrations from Canadian Forces Base (CFB) Alert in Nunavut Territory, Canada. The data is collected by Environment Canada (EC) using infrared sensor and bottle measurements and made freely available through the World Data Centre for Greenhouse Gases (WDCGG) (Trivett et al., 1994). The location of CFB Alert (82.45°N, 62.52°W) is significantly further north than data from our observing campaign (56.8°N, 52.2°W), but because CO_2 is a well-mixed greenhouse gas (Lacis et al., 2010) it serves as a good first approximation. We converted molar fraction data to wet atmospheric pCO_2 using atmospheric pressure, correcting for the saturation

vapour pressure of water near the ocean surface according to Goff (1957), following Wanninkhof and McGillis (1999).

$$pCO_{2,Air} = xCO_2(P_{atm} - P_{H_2O}) \qquad (3.1)$$

There were no direct meteorological observations within a 200 km radius of the observation site during the VITALS deployment in the Fall of 2016. Therefore we used a reanalysis product to infer variables such as 10 m wind speeds (U_{10}) and sea level pressure (P_{atm}). Moore et al. (2008) showed good agreement between North American Regional Reanalysis (NARR) winds and direct buoy observations near the tip of Greenland. The reanalysis data set has a 3-hour time step and a spatial grid cell of 32 km with wind scales of 200 km (Mesinger et al., 2006). We interpolated the closest grid cells from the NARR product to match the location of the K1 and SeaCycler moorings.

3.3 Data Processing

Upon recovery of the various platforms and instruments, the entire glider data were archived with several levels of redundancy, including storage on servers online and hard drives. The processed Labrador Sea glider data are made freely available online through Coriolis Data Centre. Making data freely available online generates a more substantial impact of observing missions, contributing to other projects such as data assimilation. It also allows other user groups to verify methods and observations and potentially point out problems, strengthening the accuracy of results.

3.3.1 SeaCycler

After recovery of the SeaCycler profiler, the data collected by the individual instruments were quality checked for outliers against standard accepted ranges in seawater. Continuously profiled data (CTD and O_2) were binned on a 0.3 m vertical grid, preserving the SeaCycler platform original resolution and missing gaps of up to 3 days were linearly interpolated. The discrete Pro CV points were linearly interpolated in depth and space.

3.3.2 Glider

After recovery of the glider, the raw data files from the science and glider computer cards were converted from dinkum binary (.dbd and .ebd) to ASCII format for further post-processing using standard batch programs provided by the manufacturer. Next, we interpolated observations to an equal 5 second spaced time grid and processed the glider positions using a simple model to account for error in glider dead reckoned position between subsequent GPS surfacing positions and linearly interpolated glider data for gaps less than 5 minutes long. A conductivity (C) temperature (T) filter was used to remove outliers defined as three times outside the standard median deviation (MAD) along the straight line fit to the T-C data. Before using the glider CTD data to compute salinity, we corrected for temperature induced sensor lag in the glider pumped conductivity cell. We applied the model from Morison et al. (1994) with a sequential comparison between glider profiles for error minimization in the correction constants similar to Garau et al. (2011). We used the TEOS toolbox by McDougall and Barker (2011) with the glider conductivity, temperature and pressure data to

calculate properties of seawater such as salinity, potential temperature, potential density. To correct for the phase response lag in the glider oxygen data, we applied the model published in Bittig et al. (2014) using raw sensor phase angle output. Instead of using the built-in optode thermistor, we used the temperature readings provided by the CTD.

$$c_{i+1}^{\text{filt}} = a \cdot c_i^{\text{filt}} + b \cdot (c_{i+1}^{\text{in situ}} + c_i^{\text{in situ}})$$

$$a = 1 - 2b, \quad b = (1 + 2\frac{\tau}{t_{i+1} - t_i})$$

(3.2)

In the above formulation c^{filt} is the corrected and $c^{\text{in situ}}$ is the raw sensor reading. Corrected values are calculated at time steps $i + 1$ by setting the first corrected sensor output to the original raw sensor reading, and using this value to calculate the next values at time step $i + 1$ using coefficients a and b. These coefficients are modified by the response time τ which are temperature dependent and calculated from prior tank calibration fits or through the published model (Bittig et al., 2014). From the corrected phase readings, we computed the molar oxygen concentrations (μmol·L^{-1}) using the modified Stern-Volmer model (Uchida et al., 2008), with fit constants from a prior optode tank calibration. For the CO_2 optode, there was no previous literature available for temperature dependent response time corrections for the sensor on a moving platform. We speculated that due to the DLR technique in the foil and available field results, the sensor response would be larger than the O_2 optode, which uses more straightforward foil chemistry. To correct for the long response time behaviour, we used a sequential time-lag correction approach recently applied in Fiedler et al. (2013) for an equilibrator type NDIR gas instrument. Fiedler et al. (2013) mounted the NDIR instrument on a profiling float with response times

on the order of 100–300 seconds between surface and depth measurements.

$$c_{i+1}^{\text{cor}} = \frac{c_{i+1}^{\text{in situ}} - \left[c_i^{\text{in situ}} \exp\left(-\Delta t/\tau\right)\right]}{1 - exp(-\Delta t/\tau)} \qquad (3.3)$$

Here $c^{\text{in situ}}$ is the raw and c^{cor} is the corrected sensor output at each time step i. The time constant τ can be computed by fitting an exponential model to the sensor response $x(t)$ (Equation 3.4) using fitting constants a, b at each time interval dt.

$$x(t) = (a - b)\exp\left(-dt/\tau\right) + b \qquad (3.4)$$

Atamanchuk et al. (2014) provided a few values for response time. However, these were for temperatures much warmer than found in the Labrador Sea or Trinity Bay and did not provide response characterization for varying temperature gradients. Fiedler et al. (2013) used an exponential model (Equation 3.4) to compare his NDIR sensors response to zero-measurements (ZM). ZM is a feature of the sensor to strip the gas stream off CO_2, and the resulting reading should be zero. The time response of the sensor and resulting reading after ZM can be used to gauge the response of the sensor to smaller gas gradients and drift of the gas detector itself. Because the optode sensor does not have the internal capability for independent referencing of the foil chemistry, we fitted the equation to the sensor response, while the glider was ascending or descending through the thermocline. Repeating this procedure for both glider deployments, we computed a temperature and response time-dependent set of values. Step profiles from Trinity Bay were especially useful for extracting sensor response to a broader set of positive and negative temperature gradients. See Figure 3.3, for a least squares fit example for a single temperature gradient and optode response excursion. A MATLAB® implementation of the above optode signal fitting

and correction routines is included in Appendix B. To compute the partial pressure of CO_2 (pCO_2) in micro-atmosphere (μatm) from the sensors corrected phase readings, we applied a calibration fit model from previous tank tests as was done in previous deployments of this sensor (Atamanchuk et al., 2015; Peeters et al., 2016). A testing regime of temperature and molar xCO_2 concentrations step changes and sensors phase response readings were used to compute an 8-degree phase and 3-degree temperature model fit, which we applied to the sensor.

Step Profile September 14: Trinity Bay Deployment 2018
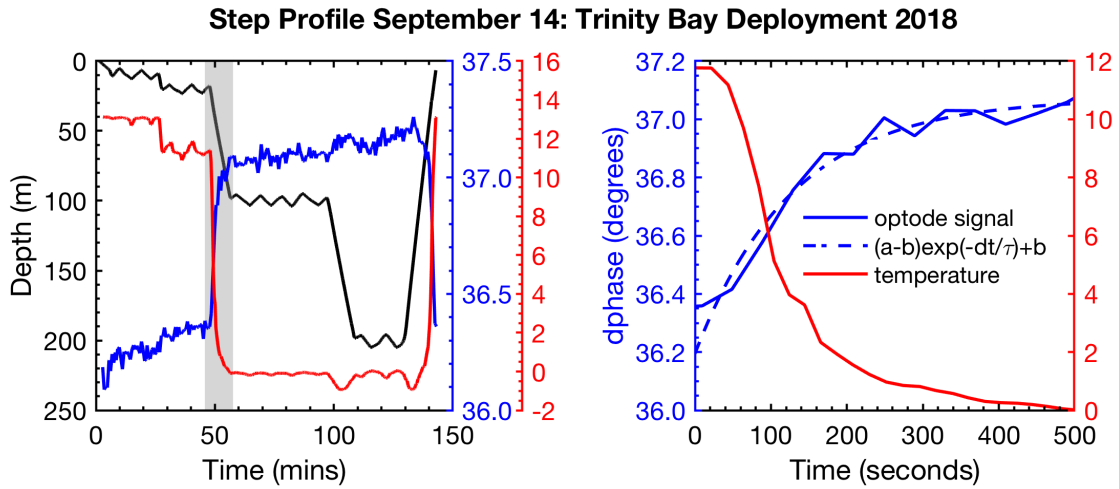
Figure 3.3: Example of a step profile used to quantify response time characteristics.

The CO_2 optode sensor underwent lengthy conditioning effects during both deployments (Atamanchuk et al., 2015). For the VITALS deployment, based on the surface SeaCycler and atmospheric data, we subtracted a linear offset to correct the drift in the sensor. A linear offset was not possible with the Trinity Bay data, and we did not correct for the offset, but instead picked the data where the drift stabilized. In the VITALS data this occurred a month into the deployment, while in Trinity Bay

tests, the sensor stabilized after a week. Such a conditioning effect is not surprising, and many electrochemical sensors such as Clark-type electrode O_2 sensors will exhibit different drift behaviour that needs correcting.

Briefly, we should mention gridding and mapping techniques utilized in this thesis for the glider data collected during the Labrador Sea mission. To visualize data, or to compare observations across platforms, we needed to bring the glider observations to an even space, time and depth grid. This was done by creating a space-time averaging scheme, which averaged data following isopycnal contours. For some cross-sectional plots, we also averaged data in depth-space or depth-time sections. To account for the gaps in observations, we preserved gaps larger than 10 km and more prolonged than 4 days. Smaller gaps were linearly interpolated. A 3D boxcar filter was applied to smooth 5 km in the horizontal, 5 m depth and 3-day in time, keeping with the observing gaps in the data because the glider occupied a section between K1 and SeaCycler every 2 to 3 days and gaps between profiles were 3 km on average. These dimensions informed the applied level of averaging.

To grid the sparse O_2 and pCO_2 glider observations for spatial-temporal data inter-comparison with SeaCycler, we deviated from linear interpolation and used an objective interpolation method using second-degree polynomial fitting distance weighting scheme following Goodin et al. (1979). We gridded the sparse data on a 1-km by a 1-day grid and then interpolating the data using an exponential weighting function $\exp\left(R_x^{-2} + R_y^{-2}\right)$ to fill in gaps. We choose influence and cutoff radius based on the number of observations in horizontal and time dimensions, which works out to influence radii of approximately 5 km for O_2 and 20 km for pCO_2 measurements and cutoffs at 10 and 40 km respectively. We set the cutoff radius as twice the spatial

scale. Temporal scales are similar between data sets with influence radius of 3 days and cutoff of 6 days.

3.3.3 Shipboard CTD and Pro CV

Following the completion of the Trinity Bay Tests, CTD profiles together with O_2 optode and data from the Pro CV were downloaded from the instruments. We converted the Sea Bird native hex file format to ASCII files and performed outlier checks on the profiles. We then read all the profiles into MATLAB$^{\circledR}$ and created a data structure. Despite the use of a pump, the Pro CV showed long signal equilibration periods (τ_{95} between 10 to 15 min). To compute the CO_2 levels for each time the CTD was parked at depth, we took the average of the CO_2-Pro CV values, once readings stabilized over 60 seconds. We developed a simple script that identified the first time window when the difference in sensor readings reached $\Delta CO_2 \leq 10$ ppm. Pro CV ZM were subtracted from bottle stops to arrive at a high-quality in-situ data set. We also calculated the standard deviation of each Pro CV measurement and flagged any data points as outliers were standard deviation exceeded 5 ppm.

Chapter 4

CO$_2$ Optode Sensor Performance

4.1 Response Characteristics

Two deployments evaluated the prototype Aanderaa Data Instruments CO$_2$ optode (Atamanchuk et al., 2014) with the more well established but slow, reference infrared-based Pro Oceanus CO$_2$-Pro CV (Jiang et al., 2014; Fritzsche et al., 2018), to advance low cost and low power in-situ marine CO$_2$ measurements from ocean gliders. The Labrador Sea deployment, as part of VITALS, was a full-scale observing mission, involving a multi-month remote ocean site deployment. Whereas, tests in Trinity Bay focused on a more controlled calibration experiment to determine sampling modes and characteristic sensor response. High-quality reference data were collected in each case: SeaCycler profiler in the Labrador Sea and ship casts in the Trinity Bay deployment, allowing for quality control assessment of glider data. Here we present results from these deployments, our analysis of the sensor performance, discuss issues and make recommendations to improve the sensor for future profiling use.

The CO_2 Optode sensor was not explicitly designed for profiling platforms such as the glider. However, it is one of only a few sensors with the low-power characteristics and size that can fit on a glider. Key to processing the sensor is to correct for the time it takes for the sensor to equilibrate (i.e. register a change) in ambient CO_2 levels. The sensor is not responsive to CO_2 concentration levels but instead responds to the change in carbonic acid levels, which causes a change in pH. The strong temperature dependence of this process requires significant time response correction in the presence of sharp temperature gradients, which occurs when crossing rapidly through the thermocline. We assess the response time, by fitting the raw sensor signal dphase sensor property (ϕ_{DLR}) with an exponential model, $x(t) = (a - b) \exp(-dt/\tau) + b$, as described in Chapter 3. Here $x(t)$ is the raw sensor signal; a and b are constants, dt is the time interval in seconds, and τ is the e-folding scale or the response time. Typically, we define the signal response time, as the time for a signal to reach a specific strength as a percentage of total true signal, we used τ_{95}, that is time to reach 95% of the total signal level. The larger the value, the longer it takes the sensor to equilibrate to ambient conditions. Given the many hundreds of vertical profiles as well as the step profiles taken during the VITALS and Trinity Bay missions, we can do a comparative analysis of the sensors response time bias against temperature gradient and initial sensor temperature. Figure 4.1 shows the result of response time fitting against the temperature gradient normalized by the total time of traversing the gradient and the sensor response (e.g. $\tau_{95,normalized} = \tau_{95}/\Delta T \times 900$). Panel 4.1a color indicates the magnitude of root mean square error (RMSE) of least squares data fitting. In panel 4.1b, color represents temperature gradient. We multiply normalized values by 900 seconds or 15 min to arrive at a set of equally referenced temperature gradient and
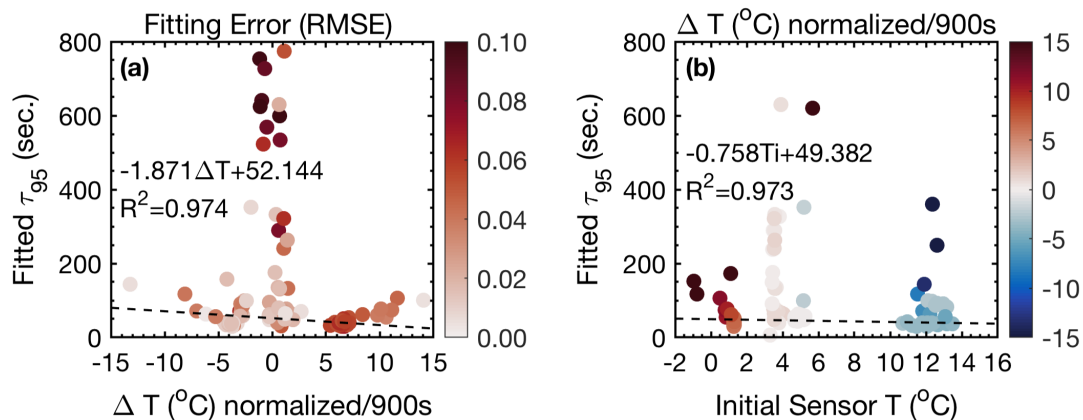
Figure 4.1: (a) CO_2 optode response time and temperature gradients colored for RMSE (b) response time and initial sensor temperature colored for ΔT.

response time values all corresponding to the same time interval. We chose this time length based on the response time ($\tau_{95} \approx 15$ min) of the reference sensing system used in the deployments, the Pro CV. We exclude RMSE errors in fits larger than 0.1 (mean is 0.0322 with a standard deviation of 0.0205). There is a strong bias in the response time between warm and cold temperatures, based on the large gradients in Trinity Bay, but we see large scatter among small gradients from VITALS data, where stratification and hence temperature gradients are smaller compared to Trinity Bay. One would expect smaller response times for smaller temperature gradients. We note here that the VITALS data shown above are mostly derived from average glider profiles (yo's), while Trinity Bay data mostly step profiles. Also, we see a small trend in initial sensor temperature on response time: that is an initially colder sensor responds better to warming than a warm sensor to cooling.

To explain the varied temperature behaviour of the sensor, we need to discuss
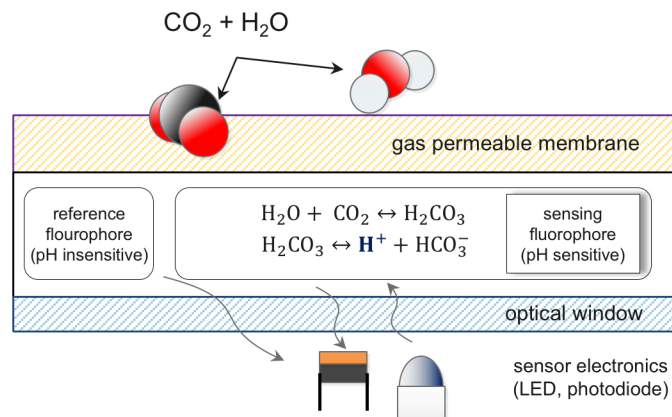
Figure 4.2: Schematic drawing of the CO_2 optode sensing foil.

the foil construction of the sensor (Figure 4.2). The CO_2 optode sensor foil does not directly react to the presence of CO_2 in the water column. Instead, the sensor foil chemistry is sensitive to changing pH levels from carbonic acid (H_2CO_3), which dissociates into H^+ and HCO_3^- ions, thereby decreasing pH. However not just carbonic acid is capable of changing pH levels in seawater (though most prominent). Therefore, the foil has a gas permeable membrane, that only allows diffusion of CO_2 (gas) to the inside part of the foil where it can form carbonic acid. Presence of a stronger acid, such as sulfuric acid (H_2SO_4) reactive to carbon, will disrupt the sensor chemistry and irreversibly damage the foil (poisoning). Below the membrane, light-activated (fluorescent) compounds are embedded inside a buffer solution, chemically sensitive to changing levels of pH due to carbonic acid increase or decrease. This change is recorded by the sensor as a shift in the lifetime of excitation response from the fluorophore (or luminophore) based on a reference chemical not sensitive to pH. The exact chemicals used for the fluorescent compounds are not mentioned in Atamanchuk et al. (2014), but it is likely hydroxypyrene trisulfonate (HPTS). This compound is

most widely used as a pH-sensitive fluorescent indicator but has low sensitivity and brightness compared to other alternatives currently being developed (Fritzsche et al., 2017). This means there are several rate-limiting processes which must first occur inside the foil before the sensor can register changing levels of CO_2, the sum of which contribute to the total response and sensitivity of the sensor and are temperature dependent. Here we discuss each step in the process to draw a broader conclusion about the sensor design, referencing pertinent laws in chemistry.

The first rate-limiting process of the sensor is the rate at which gas can diffuse through the sensor foil membrane. This rate is governed by Fick's First Law (Fick, 1855).

$$J = D\frac{\partial CO_2}{\partial x} \tag{4.1}$$

This relationship (4.1) states that the net diffusion D in units of mol·m^{-2} s^{-1} is proportional to the substance gradient across a boundary, in this case, the membrane thickness x or $\partial CO_2/\partial x$ and the diffusivity of the substance D, which is temperature dependent (increasing with temperature in Arrhenius equation). In other words, membrane thickness contributes inversely to the diffusion rate, while increased temperature increases the diffusivity of the gas. As gas diffuses through the membrane, it then has to undergo a two-step process inside the foils buffer to form carbonic acid and dissociate into HCO_3^- and H^+ protons which induce a pH change in the buffer (Figure 4.2). Two separate processes, the rate of which is temperature dependent.

$$k = A\exp\left(-\frac{E_a}{RT}\right) \tag{4.2}$$

Equation 4.2 is the Arrhenius Equation (Arrhenius, 1889) which shows exponential dependence between the reaction rate k and absolute temperature T (Kelvin). Finally,

the fluorophore (we assume it is HPTS) has to respond to the changing pH levels and exhibit a changing signal intensity due to the modulating blue light. The sensors photodiode has to then detect the difference in lifetime between the fluorophore and its reference. We assume that this third step is less affected by temperature, compared to the first two processes. The reaction with the fluorophore continues as the first two processes (diffusion and chemical reaction) slowly equilibrate buffer to ambient pH levels. Therefore the fluorophore response time is not an independent variable, but instead intrinsically coupled with the first two steps. The time response of internal sensor electronics (milliseconds) is virtually unaffected by temperature compared to the time constants of the first two processes (hundreds of seconds).

While processing the glider deployment data, we looked at response time trends of the sensor profiling through weak and strongly stratified water bodies and found non-trivial temperature-dependent behaviour, which we explained through careful reasoning of the foil construction. In summary, the temperature behaviour of the sensor should lead to discernable differences between glider data from mostly profiling modes and just data from step profiles. If we superimpose measured raw CO_2 optode sensor output with high-quality temperature, salinity and absolute CO_2 measurements from the CO_2-Pro CV, we should be able to see different response characteristics not captured in Figure 4.1. For temperature and sensor response time we expect to see a fairly linear response, as the solubility of CO_2 in seawater is reasonably linear (Weiss, 1974) over small temperature ranges (ΔT less than 10°C). The unique step profile casts from the Trinity Bay deployment allow an investigation into sensor stability and equilibration, compared to normal glider profiling modes. To match records between observations, we use isopycnal matching, averaging recorded data over bin sizes of
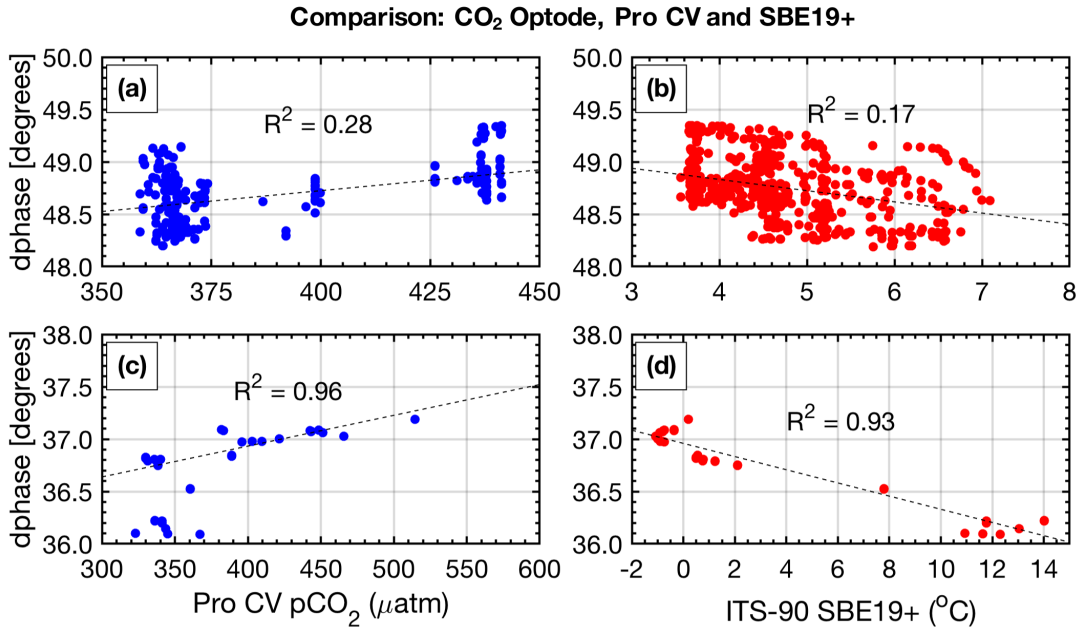
Figure 4.3: CO_2 optode signal plotted against VITALS (a) absolute CO_2 measured by the Pro CV on SeaCycler and (b) temperature from SBE 19+. Panels (c) and (d) show Trinity Bay step profile data plotted against shipboard measurements. Dashed lines are linear fits.

0.01 kg/m^3. Figure 4.3 indeed, shows noticeable differences in the glider CO_2 optode data between the two deployments. In the VITALS data shown above, for which we primarily used regular glider profiling, the scatter is much larger among temperature dependence of the response, while in Trinity Bay data, which relied on step profiles, this scatter is much reduced. The longer time for the sensor to equilibrate increases the linearity of the sensor response, reproducing the mostly linear relationship between CO_2 solubility and temperature. For the VITALS data, we see a linear trend among the scatter data, but clearly, the amount of scattering was not corrected through our methods giving a broad range of possible CO_2 values for a given temperature in the

calibration model.

In summary, this three-step process which must happen to detect changes in CO_2 is complicated. Each step is temperature dependent making this CO_2 sensing process complicated. Therefore, we expect to see some substantial variability in sensor response during profiling applications, and this can explain the more considerable scatter of response time observations. Some of these rate-limited time response problems could be reduced, for example, by decreasing the membrane thickness, but that could severely impact sensor stability. In fact, testing with thinner foils (data not shown) showed that the sensor was overcome by too much sampling noise to discern any real signal in CO_2. Fundamentally the design and the problems found in regular glider profiling warrants further improvement to the sensor foil, to make the optode more robust and reliable in ocean deployments.

4.2   Comparison with SeaCycler Observations

A novel component of the VITALS mission was the use of multiple platforms to improve space and time measurements of O_2 and CO_2. As laid out in introductory chapters, an essential requirement to ocean observing between mobile platforms is that the data must be coherent: it needs to match. This ensures that the data between platforms is compatible and can be used to extend the observations of one platform using the other. As discussed in Section 2.4, glider-based observations have many platform and sensor specific challenges. The easiest way to achieve quality control in this mission was to use the high-quality SeaCycler data to cross-check and calibrate the sensors of the glider. Here we present data comparisons, time and spatial

evolution of SeaCycler-glider matched data and spatial anomalies of glider data.

4.2.1 Glider and SeaCycler O_2 and CO_2 Data

In order to compare data across ocean platforms, one should consider the water parcels measured by the sensors on each platform. Water properties in the ocean are conserved along equal density contours in T-S space, and one should not merely use temperature or depth to relate observations. This is especially important to consider in the Labrador Sea, where strong oscillations can shift the apparent depth of density surfaces by hundreds of meters (Gascard and Clarke, 1983). Therefore, density (isopycnal) comparison were used to find matching glider and SeaCycler data. We binned data for the glider observing period (3 October to 22 November) in equal density bins of 0.01 kg/m^3, with 1-day resolution and computed temperature and salinity residuals from both data sets. If temperature matched to within 0.5°C and salinity to within 0.1 PSU, we allowed these residuals for further comparison between platform gas observations. The 95% Confidence Interval (CI) is defined as CI = $\bar{x} \pm 1.96$ STD, where $\bar{x}$ is the average of the variable of interest (e.g. pCO$_2$) and STD is the sample variance.

Following extraction of O_2 and CO_2 data across the matching observed density and time range of the two platforms, we plotted the residual cloud across density and found strong dual trends marked by the 27.56 kg/m^3 isopycnal. This isopycnal is consistent with the mean mixed layer deep (MLD) density surface as one would expect different mixed and intermediate depth water properties. We used linear-least squares fits to compute the mean correction of the glider data required to match
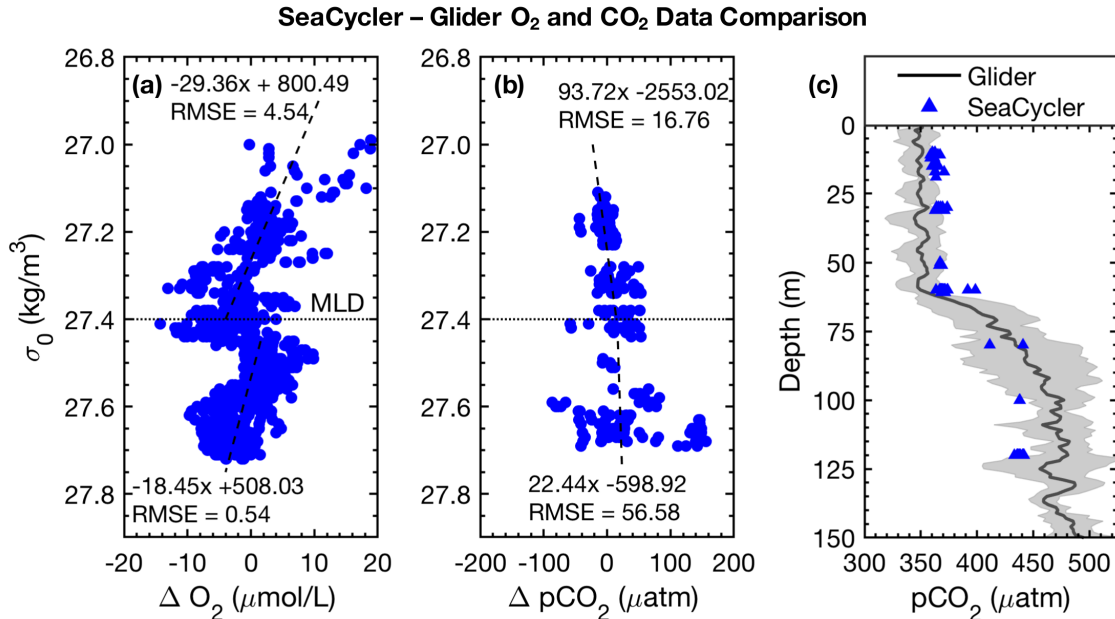
Figure 4.4: Glider-SeaCycler (a) O_2 and (b) pCO_2 isopycnal-matched residual comparison. Panel (c) shows Glider-SeaCycer corrected depth-averaged pCO_2 values with glider 95% CI shown as grey shading for the period from 3 October to 22 November 2016. Blue triangles are SeaCycler measurements. Dashed horizontal line in panels (a) and (b) is the average density of the mixed layer and dashed lines are linear fit to the residuals in density space.

the SeaCycler (Figure 4.4 indicating trends above and below MLD). More significant scatter (± 50 μatm) is observed in CO_2 residuals in at depth isopycnals below the mixed layer. Applying the residual fits from the SeaCycler–glider CO_2 offsets to the glider data (Figure 4.4c), we see reasonable agreement in the mixed layer. Below the mixed layer, the correction does not fall within the 95% CI limit. However, we see good agreement and relatively narrow spread (± 10 μmol/L) of O_2 data between SeaCycler and glider sensors leading to a good in-situ correction.
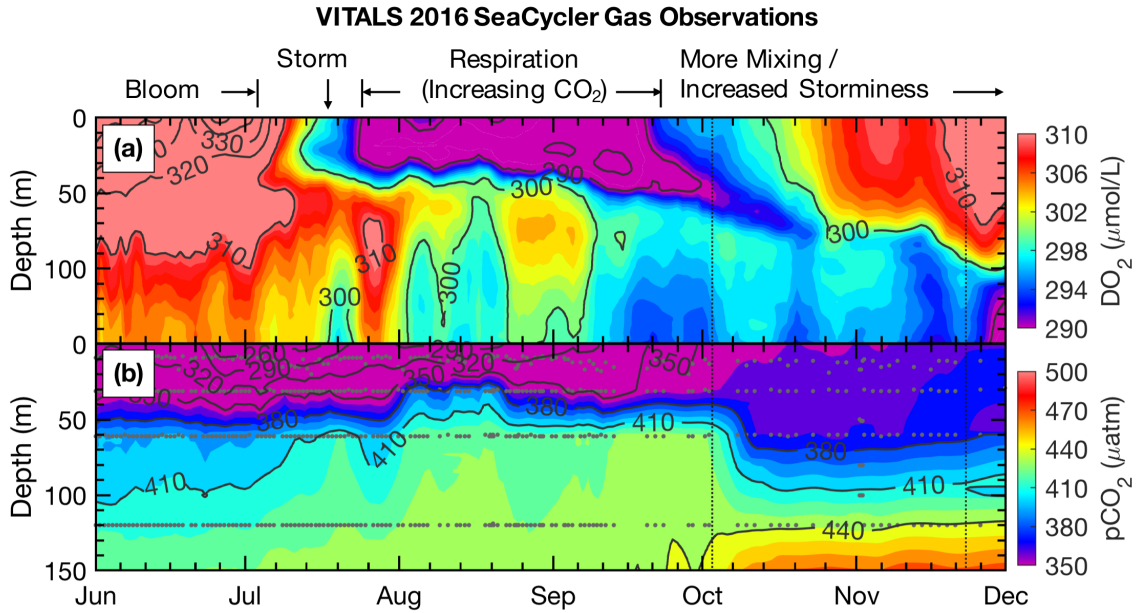
Figure 4.5: SeaCycler time evolution of (a) O_2 and (b) pCO_2 Observations.

Applying the above residual fits to the glider data we arrive at matching in time-depth-space platform data set that can now be used to analyze horizontal anomalies. First, however, we describe the context of the spatial and temporal observations between both platforms. Figure 4.5 shows SeaCycler gas observations. Black dotted lines indicate the start and end of joint sampling period with the glider. Small grey dots are the depth and time of discrete Pro CV measurements by the SeaCycler. The record is divided into periods of increased biological productivity, CO_2 respiration from bacteria due to settled summer biological productivity and storms. Generally, the fine detail of SeaCycler surface observations in time is astonishing. June to August shows a pronounced increase of O_2 levels due to surface biological productivity, with low pCO_2 at depth during the same time. A mixing storm-like event separates this phase with a sharp gradient of much-decreased surface O_2 levels from August to

60

October. At the same time, CO_2 values increase at depth, due to the respiration of bacteria attracted towards the end of the spring/summer bloom. In early October, increased storminess mixes the surface layer, increasing O_2 and pCO_2. Fine details in O_2 data are visible such as inversions and subduction of lower O_2 levels. Overlaid with these biogenic factors are also solubility driven changes, leading to increasing O_2 in a deepening mixed layer as temperatures in the surface decrease.
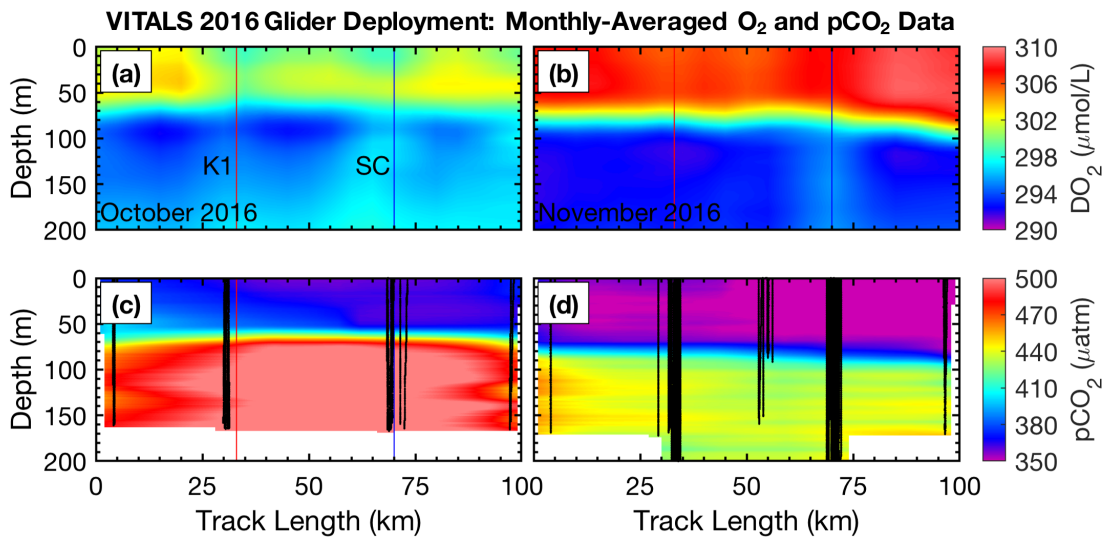
Figure 4.6: Glider monthly averaged spatial section of (a) O_2 in October and (b) November and pCO_2 respectively (c) and (d) indicating location of K1 and SC moorings. Black lines (c) and (d) are locations of glider pCO_2 profiles.

The glider, corrected to the SeaCycler observations, sees spatial snapshots of the processes captured by SeaCycler in time. Figure 4.6, shows monthly averaged panels (approximately 10 glider passes distance-averaged per month) of the glider gas data. Along-track location of K1 mooring and SeaCycler are indicated with vertical lines as well as individual CO_2 optode glider profiles used for plotting. The much lower

spatial density of CO_2 glider profiles compared O_2, means that the CO_2 data resolves only spatial features with scales larger than 20 km, compared to a 5 km resolution for O_2. Overall, this region is relatively uniform, with low spatial gradients. Consistent with the SeaCycler observations, we see a flip between concentrations in O_2 and CO_2 between October and November. We also note the different thickness of mixed layer regions across the spatial domain in November. Smaller pockets of low or high O_2 concentrations exist in October, but these trends are weak in an average sense.

4.2.2 Spatial and Temporal Anomalies

Using the glider record, we can look at how representative the SeaCycler time series was along the 100 km horizontal distance trajectory sampled by the glider for the two months while near SeaCycler and K1. We average the glider data top 20 m and grid this surface mixed layer over the 100 km and 50 days (3 October – 22 November) long track record, subtracting SeaCycler 20 m surface average time trend from the glider data to look at spatial and temporal trends in O_2 and CO_2. We applied the objective interpolation technique described in Section 3.3.2, interpolating the data using an exponential weighting function to fill in gaps. We could have used linear interpolation for the glider oxygen data but decided to keep mapping methods consistent between O_2 and pCO_2 data. A drawback with this technique is that it can show artificial variability in the resultant interpolated surface. Results are shown Figure 4.7 and Figure 4.8. Dots indicate the location of data samples. The legends in the below figures, only mask data where no glider data was collected.

From this analysis, we see that there are a few spatial features visible in O_2 data.
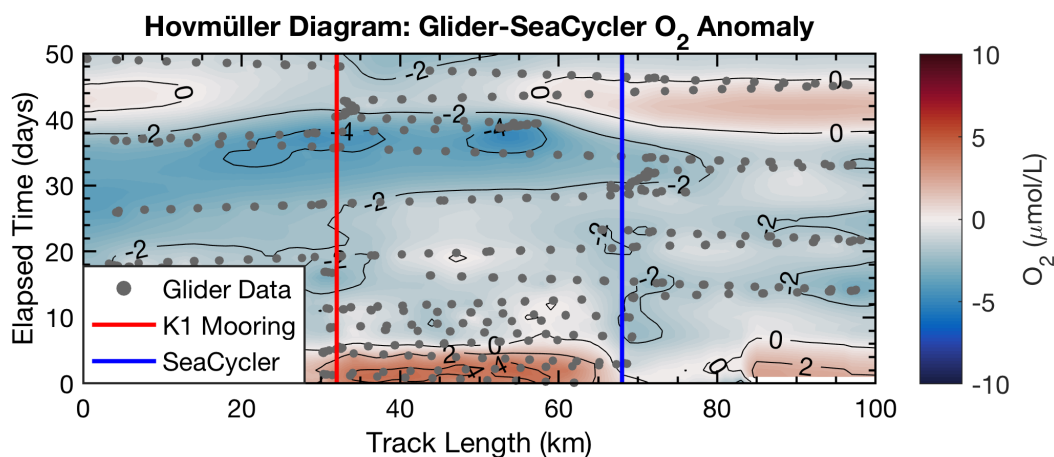
Figure 4.7: Glider Hovmüller diagram, for O_2 data (top 20 m) with SeaCycler data removed for period 3 October – 22 November, 2016. Dots indicate the location of data samples. Legends mask area where no glider data was collected.
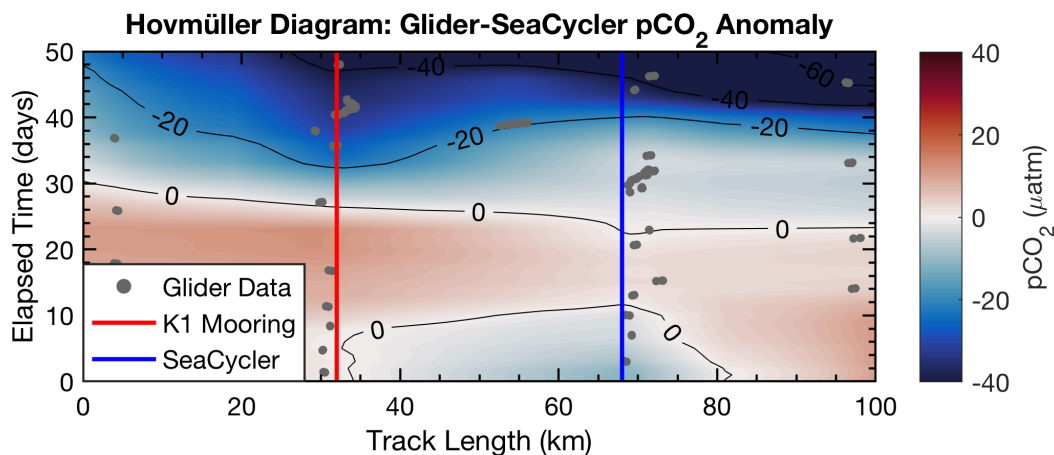
Figure 4.8: Glider Hovmüller diagram, for CO_2 data (top 20 m) with SeaCycler data removed for period 3 October – 22 November, 2016. Dots indicate the location of data samples. Legends mask area where no glider data was collected.

However, the overall spatial structure is not as pronounced as time variability. Towards the beginning of the record, there is a distinctly more oxygenated zone between

63

K1 mooring and SeaCycler. This could mean that perhaps the low oxygen levels measured by SeaCycler from August to October had more considerable spatial variability. The beginning of the glider record, also shows an intense mixing event, perhaps an eddy, described in Section 5.1.1. There are different patterns between moorings. Near SeaCycler the O_2 levels are somewhat higher compared to K1 mooring, while data near K1 mooring shows lower oxygen features over time. Towards the second half of the glider record, as storm activity increases in November, the spatial domain becomes more smooth. As described in the mission summary in Section 3.3.2, the glider sampled O_2 daily and along the entire track length, while the CO_2 optode was only sampled at select locations and on average every 2–3 days. The CO_2 glider data sampling was too sparse and required too much smoothing from interpolation to resolve signals smaller than the seasonal cycle. Therefore, the data appears very uniform along the track length. However, this type of direct comparison between platforms will become increasingly important in future glider deployments to achieve long term monitoring capability, recalibrate sensors and to quality control mobile platform data.

Chapter 5

Labrador Sea Glider Observations

5.1 Stratification, Spatial and Temporal Scales

The unique mission, location and resolution of the glider data warrants its own section to investigate the data and characterize hydrography, both spatial and temporal trends as well as the variability of the measured parameters. Building on the Labrador Sea oceanography discussion in the background chapter and careful investigation, this section reviews various events captured by the glider and attempts to characterize and describe them.

5.1.1 Stratification

In the Labrador Sea, density stratification becomes strongest at the end of summer and early fall. Sea ice melt and heat from the sun cause the formation of the strongest gradient in salinities between the surface mixed layer (between 40 to 100 m deep) and intermediate depth waters (200 to 900 m). As the season moves towards autumn,

cooling and stirring of the water from storms homogenizes the surface mixed layer. The glider data reveal a definite increase in the surface mixed layer depth (surface
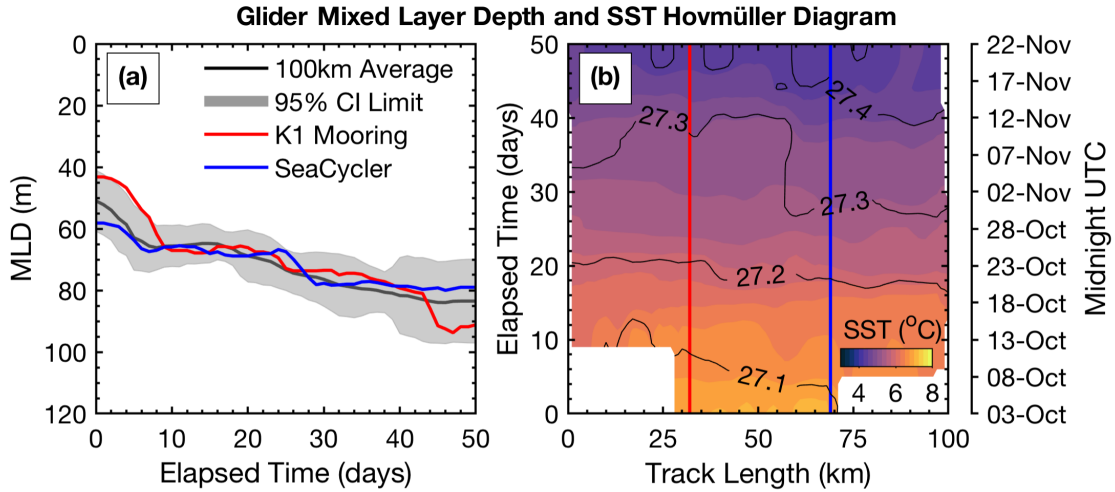
Figure 5.1: Mixed layer depth (a) and (b) surface temperature evolution for the observation period with density surface outcrop contours shown.

mixed layer depth defined as $z > 20$ m & $d\sigma_0/dz > 0.01$ kg/m^3). Over 50 days, we see a deepening of almost 40 m, which is equivalent to an increase in surface mixed layer depth of 0.8 m·day^{-1} (Figure 5.1). We see that the mixed layer deepening is not exactly uniform over the spatial and time domain of the glider data. Grey shading in Figure 5.1a indicates the 95 CI, using the same definition as in Section 4.2.1, where the variance is normalized by the entire data sample to compute the sample deviation. Red and blue lines show glider time series at SeaCycler and K1 mooring location for reference.

During the glider 50-day record, several strong mixing events stand out. One particular event was captured early in the glider deployment (7 − 9 October), ap-

proximately 10 km South-West from K1 mooring, changing vertical temperatures by almost 1°C at a depth greater than 800m in a day. This event has the characteristics of an eddy (mixing depth, time scale and water properties), but insufficient spatial and temporal data is available to fully classify this event as an eddy. Across all
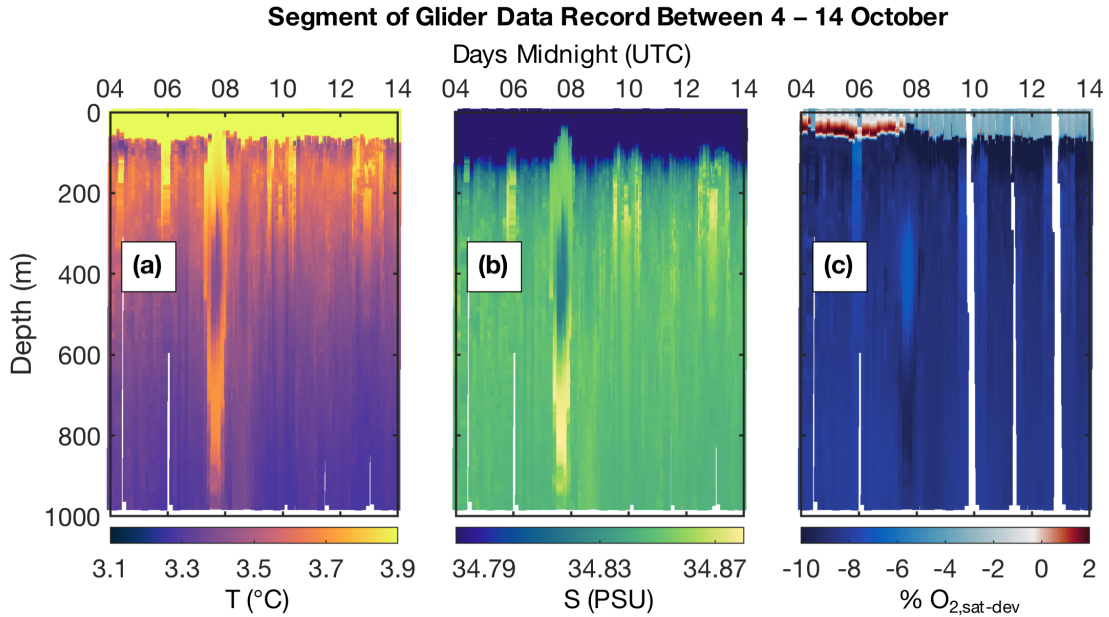
Figure 5.2: The glider captured a strong eddy-like event. Panels have dates indicated as midnight UTC (top axis) for (a) temperature, (b) salinity and (c) O_2 saturation deviance referenced to 100% solubility.

measured properties of the glider (except pCO_2 as the optode was turned on only a fraction of the time), we see a strong change in intermediate water properties (Figure 5.2). In Figure 5.2, T–S color is adjusted to intermediate depth water properties. The event only lasted a few days, while the glider was slightly outside its normal straight line transect course and spatially the eddy-like event was less than 10 km

wide. Remarkable changes are also visible in the oxygen saturation deviation from 100% saturation with respect to solubility ($O_{2,\text{sat-dev}}$), which we define as:

$$O_{2,\text{sat-dev}} = (\frac{O_2}{O_{2,\text{sol}}} - 1) \times 100\% \qquad (5.1)$$

were O_2 is measured and $O_{2,\text{sol}}$ is the solubility of oxygen (Garcia and Gordon, 1992), implemented as part of the TEOS Toolbox (McDougall and Barker, 2011). This form of oxygen saturation equation, explains the ratio of O_2 in terms of under or over-saturation compared to 100% saturation. Before the event, the mixed layer was slightly oversaturated (2%), but after the event had passed, saturation dropped -4% for the mixed layer, and over -10% below the mixed layer.

We can assess the mixing depth strength or stratification stability directly through assessing the cumulative difference in density between intermediate depth and the vertical water column above it. This quantity termed Convective Resistance (CR), measured in kg/m^2, was proposed in Bailey et al. (2005) and implemented by Frajka-Williams et al. (2014) to study differences in horizontal stratification in the Labrador Sea for a glider deployment. A negative CR indicates stable stratification, while a CR of 0 would mean a well mixed or homogeneous layer and a positive CR would mean the water column is unstable. This method essentially assesses the amount of buoyancy that needs to be removed to achieve a homogeneous water layer where downward mixing can occur. We apply the same method to our glider data to quantify vertical stratification and changes over time.

$$\text{CR}(h) = \int_{-h}^{0} \sigma_1(\text{S}, \theta, z)dz - h\sigma_1(\text{S}, \theta, h) \qquad (5.2)$$

Here σ_1 is the potential density with respect to 1000 dbar as a function of salinity (S), potential temperature (θ), and depth (z). The definition for CR(h) as a function

of depth requires one to establish a depth h at which water becomes stratified. The glider deployment analyzed in Frajka-Williams et al. (2014) was in the winter time and stratification was very low, reaching mixed layer depths of 700 m and beyond. The fall glider deployment observed mixed layer depths up to 120 m, except for the eddy-like event, that mixed water to depths of 800 m. We choose a depth of 150 m, knowing that all water below this depth was stratified. We extract all glider profiles deeper than 300 m and interpolate them to 1 dbar pressure grid and apply the above equation to compute CR. Keeping with Frajka-Williams et al. (2014) we do not change units to energy per unit volume (Bailey et al., 2005). Applying the method to
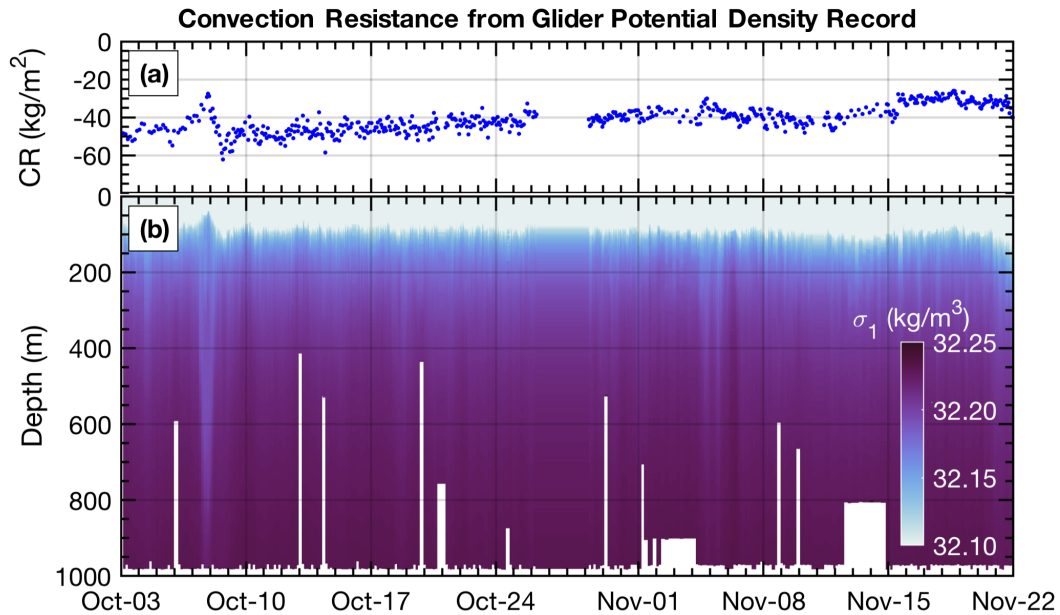
Figure 5.3: Computed Convective Resistance (a) and (b) potential density with respect to 1000 dbar (σ_1) for the glider observing period.

our glider data reveals that the passing eddy-like event had a strong impact on water

stratification, lowering stratification by more than $10\,\mathrm{kg/m^2}$ and then stabilizing water column stratification by an additional $10\,\mathrm{kg/m^2}$, before settling to former levels. No further events are visible in the glider record that had such sharp mixing, yet short time scale impact. Towards the end of the record, stratification levels reach close to the wintertime levels observed in Frajka-Williams et al. (2014). The impact on CR observed from this single event connects to the discussion in Lilly and Rhines (2002) who observed 1000 m eddies and pointed out their role in water heat loss regulation and restratification.

Besides the eddy-like event, we see a strong movement of certain density layers in the glider record, namely at intermediate depths. This layer is above previous convection formed Labrador Sea Water, but several hundred meters below the surface mixed layer. Gascard and Clarke (1983) suspected that the low stratification in the water column (e.g. gradients of $\sigma <0.1\,\mathrm{kg/m^3}$ over 100 m) below the mixed layer could harbor strong oscillations near the buoyancy frequency, the Brunt-Väisäla Frequency. (Väisäla, 1925; Brunt, 1927). The spectra of our density time series (here we switch to σ_0, which is the potential density with respect to 0 dbar) are computed by taking the first derivative of the isopycnal depth time-series with respect to time and computing the Fourier Transform power spectrum, using a window size of 1/3 the time series length (approximately 17 days). We compute the local buoyancy frequency (N^2) for the intermediate depth ($h = 200$ m) glider data ($N = 6.57 \times 10^{-4}\mathrm{s}^{-1}$).

$$N^2 = \frac{g}{\sigma_0(h)}\frac{\partial \sigma_0(z)}{\partial z} \tag{5.3}$$

In the above formula g is gravity, $\sigma_0(z)$ is potential density to 0 dbar at depth z and $\sigma_0(h)$ is potential density at reference depth h. We notice distinct peaks in

Select Isopycnal Slope Spectra from VITALS Glider Record
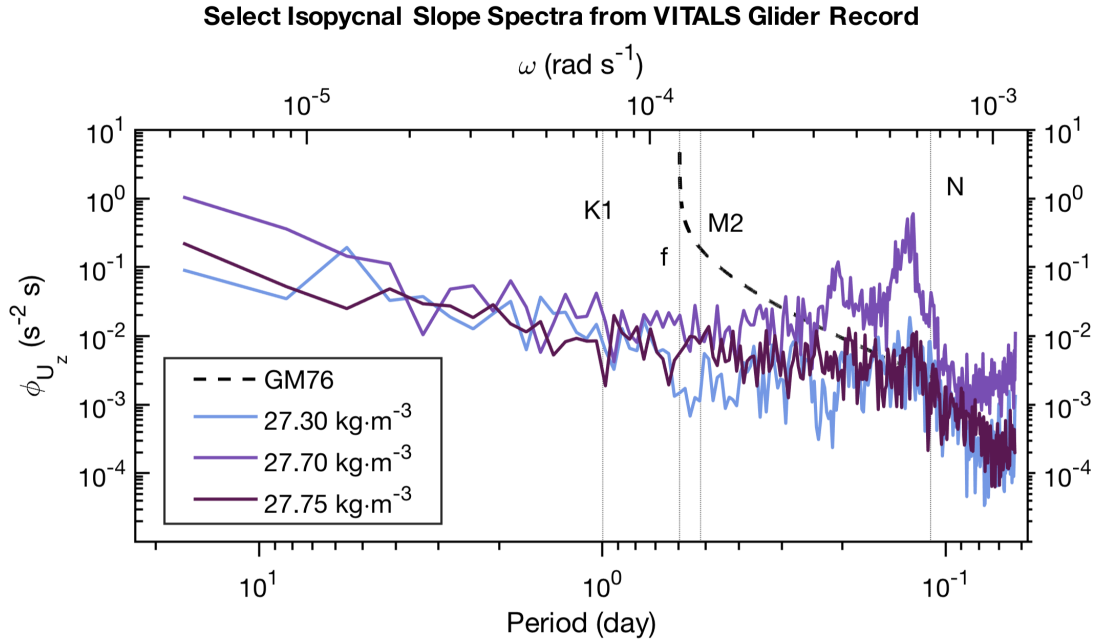
Figure 5.4: Frequency spectra of selected along isopycnal (σ_0) depth–time series. Dashed line is the Garret–Munk (GM) 1976 internal wave frequency spectrum as modified by Cairns and Williams (1976). Major tidal components (K1 and M1), Coriolis (f) and Brunt-Väisäla Frequency (N) are shown with dotted lines.

intermediate depth isopycnal range from 27.7 to 27.73 kg/m³ which occupies depths from 200 to 800 m. These peaks have reoccurring energies at roughly 3 and 5 hours. Overlaid with the Garrett-Munk (GM) internal wave frequency-spectrum (Garrett and Munk, 1975) modified by Cairns and Williams (1976) (known as GM76), we see energies (peaks) present in the internal wave range between Coriolis and buoyancy frequency cutoffs. Isopycnal layers above 27.75 kg/m³ do not show the same peaks nor does the surface ($\sigma_0 \leq 27.63$ kg/m³). Diurnal and semidiurnal frequencies, as well as the Coriolis parameter and buoyancy frequency cutoff, are indicated with vertical lines. The bandwidth in peaks agrees with findings in Gascard (1973) who found the

presence of distinct peaks in the internal wave range near buoyancy frequency range from float data. The presence of energy in this range (close to buoyancy) fits into the discussion from Gascard (1973), who suggested that the buoyancy oscillations can be the cause for energy imbalance triggering sudden turbulent plumes in deep convection phase in the winter period when cold, dry winds increase wintertime heat loss.

We note that there are several limitations to the data resolution, as discussed in Chapter 3. The glider repeated transect around every 3 days and horizontal gaps of over 3 km between repeat observations, makes neither dimension sampled well enough to separate time and space processes. In addition, there is another cutoff frequency from the CTD, which was sampled every 5 seconds, with a Nyquist frequency of 2/5 or 0.4 Hz. We are mindful of the glider yoyo cycling of roughly 16 cycles per day or periods of about 1.5 hours between consecutive depth observations and shorter time scales cannot be resolved and become aliased. Therefore we can not attribute energies to particular events and can only highlight in general the presence of energies in certain frequency ranges. Next discussed are correlation scales, using correlogram techniques. This will help highlight the differences in scales between density layers in space and time.

5.1.2   Spatial and Temporal Correlation

Gliders inherently combine both spatial and temporal variability and separating one from the other is tricky. However, we can treat each as independent components and compare their autocorrelation ranges against each other as a measure of the variability observed. Chatfield (1998) provides a convenient form of the correlogram

or autocorrelation $(r(k))$ as a function of lags k.

$$r(k) = \frac{\sum_{t=1}^{N-k}(x_t - \bar{x})(x_{t+k} - \bar{x})}{\sum_{t=1}^{N}(x_t - \bar{x})^2} \tag{5.4}$$

Here, x_t denotes any quantity of interest (e.g. temperature, salinity or O_2) and $\bar{x}$ is the average of x_t along dimension t, k can denote either spatial or temporal lags and N is the total number of samples along each dimension. We map temperature, salinity and O_2 data on a space-time density grid and detrend the data to remove non-stationary time and spatial trends following the discussion from Chatfield and compute the autocorrelation in space and time lags (km and days) for salinity, temperature and O_2. We use density coordinates because otherwise, the correlation function will approximate the spectral analysis (Figure 5.4) and yield correlation values that approach some number of the period between buoyancy oscillations aliased together with spatial propagation modulated by other propagating features. Keeping consistent with the previous section, we select the density contours 27.3, 27.7 and 27.75 kg/m³, corresponding closely to surface, intermediate and deepest water regions surveyed by the glider. The autocorrelation function for temperature, salinity and O_2 (Figure 5.5) shows different spatial and time scales across all properties between surface and deeper water layers. In the above figure, temperature and O_2 have similar spatial first zero crossings of approximately 10 km for intermediate and deep waters (27.7–27.75 kg/m³) and 5 km for surface mixed layer waters (27.3 kg/m³). Salinity has first zero crossings of about 7 km for intermediate and deep layers and 13 km scales at the surface mixed layer. Time scales also vary across properties. Temperature and salinity have similar temporal correlation at the surface (13 days) and in intermediate–deep waters (7 days). Oxygen, on the other hand, has very different scales compared to T
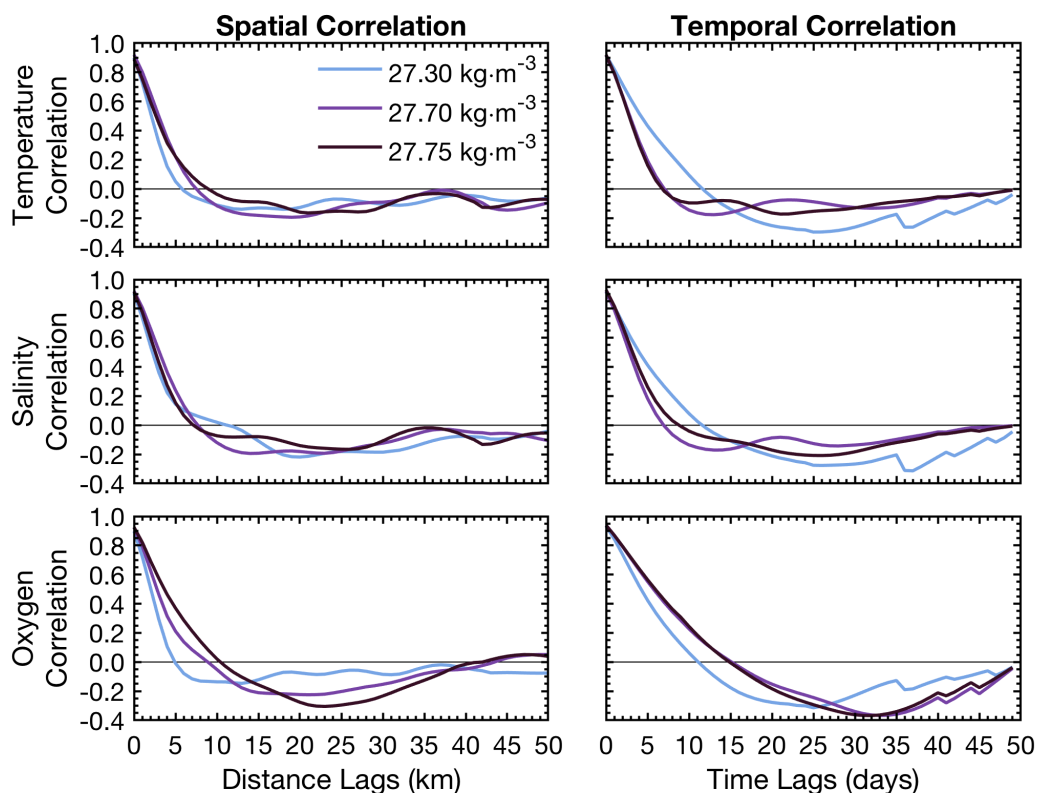
Figure 5.5: Autocorrelation functions for T, S and O_2 in space and time lags.

and S, with surface scales around 12 days and intermediate–deep water scales of 15 days.

These results suggest that there are different underlying dynamics between surface and intermediate–deep water layers that drive T, S and O_2 time scales. However, spatial scales vary less dramatically between density layers and across properties. The small spatial scales are consistent with the results from the previous section. The presence of The presence of energetic shifting of density layers (every 3 to 5 hours) in the intermediate depth waters would force spatial scales to be small. The glider takes about 3 hours to complete a full dive-climb cycle with a distance of 3 km. As the glider begins the next dive-climb cycle, the glider will likely see a shift in the

depth of intermediate depth density layers as it will be between 3 to 5 hours since it first measured the same density layer.

To explain the main driver of the time scales, we turn to a study by Sathiyamoorthy and Moore (2002) who looked at buoyancy fluxes from OWS Bravo data. This study also found similar time scales of T and S around two weeks at the surface. Their explanation links correlation scales in T and S to cyclonic air flow regime changes in the North Atlantic, suggesting storm activity at a period of roughly two weeks in the Labrador Sea in the fall. This result indicates that storms, occurring every two weeks are primarily responsible for changes in T, S and O_2 in the surface layer. The significant difference in time scales between T–S (7 days) and O_2 (15 days) across intermediate-deep layers, however, is not intuitive. A possible explanation could be the presence of biological activity that affects O_2 at intermediate depth layers, but not T and S. A 2–week period of changes in productivity could be possible, but without further insights from direct observations into the fall and early winter in the Labrador Sea, we can not be sure. As in the previous section, we must note that neither time nor spatial scale results can be interpreted without being mindful of the limitations of the glider platform due to aliasing. However, compared to contemporary studies in other water regions, our scale results point to much higher variability across all properties along time-space dimensions in the Labrador Sea.

5.2   Variability in Glider O_2 and CO_2 Observations

Variability is a key question for gas observations in the Labrador Sea. The previous subsection looked at a statistical textbook method to investigate the correlation,

while the previous chapter assessed the limitations with which gliders and optical sensors can resolve the fine-scale structure. One way to investigate the variance of the observations to the ambient surroundings is to separate data by water parcels (e.g. salinity and temperature) and look at the amount of variance in each parcel of water or water mass. This approach allows one to look at the differences in water properties (T–S) along equal density contours. In a perfect two-layer-system with large scale motions, the properties across each parcel should be very uniform with a small amount of spread, closely resembling an S-curve in T–S space. The presence of different interfering dynamics will increase the spread and size of the T–S diagram with groups or clusters of T–S properties surrounding dominant water masses, for example, Labrador Sea Water (LSW), but not as constrained to one particular curve-shape. Here we discuss the VITALS glider observations using two types of T–S diagrams, one for surface and one for subsurface scales. The difference in scales between the surface and intermediate depth layers is evident from the correlation analysis. Here we bin the glider O_2 and pCO_2 observations into bins of 0.1°C and 0.01 PSU for the surface data (Figure 5.6) and 0.01°C and 0.001 PSU for subsurface data (Figure 5.7). Across each water parcel or bin, we can compute the mean and standard deviation of associated O_2 and pCO_2 values (right panels in the figures). Note, we use potential temperature (θ_0) with respect to 0 dbar , instead of observed in-situ temperature (T).

In the diagram, for surface T–S properties we see larger scatter in less dense water layers as they are subject to strong atmospheric forcing, but also have fewer repeat glider observations. Towards depth (greater density) variance increases in each bin, because the water properties are more constrained in T–S space and data from a

76
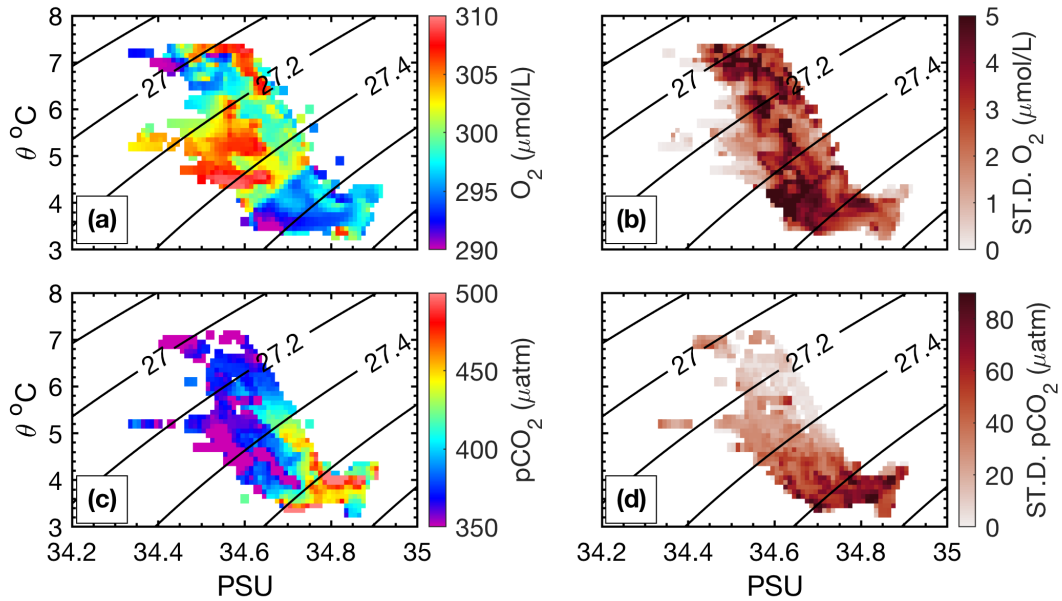
Figure 5.6: T–S diagram with isopycnal contours (σ_0) as black lines, color-coded for (a) surface O_2 and (c) pCO_2 observations and sample standard deviation (b) and (d) for each bin of O_2 and pCO_2 observations respectively.

longer time range are averaged together. In both O_2 and CO_2, colors follow a bent shape across density lines, showing seasonal-like cooling induced changes during the two months of observations. Some along-density color changes occur in O_2, which can indicate biogenic factors. Looking at depth, we see the variance for O_2 decrease and that the dominant O_2 properties follow seasonal cooling and freshening lines across density contours. The eddy-like event is clearly visible in the O_2 T–S data (Figure 5.7) as an exaggerated stump, just below the $\sigma_0 = 27.7$ line, at 34.82 PSU. The pCO_2 optode, which had much more noisy data, does not indicate trends as well as O_2, but the upside down U-shape shows seasonal-like cooling trends. However, no eddy-like signature is visible in pCO_2 as the sensor was not turned on during the event.
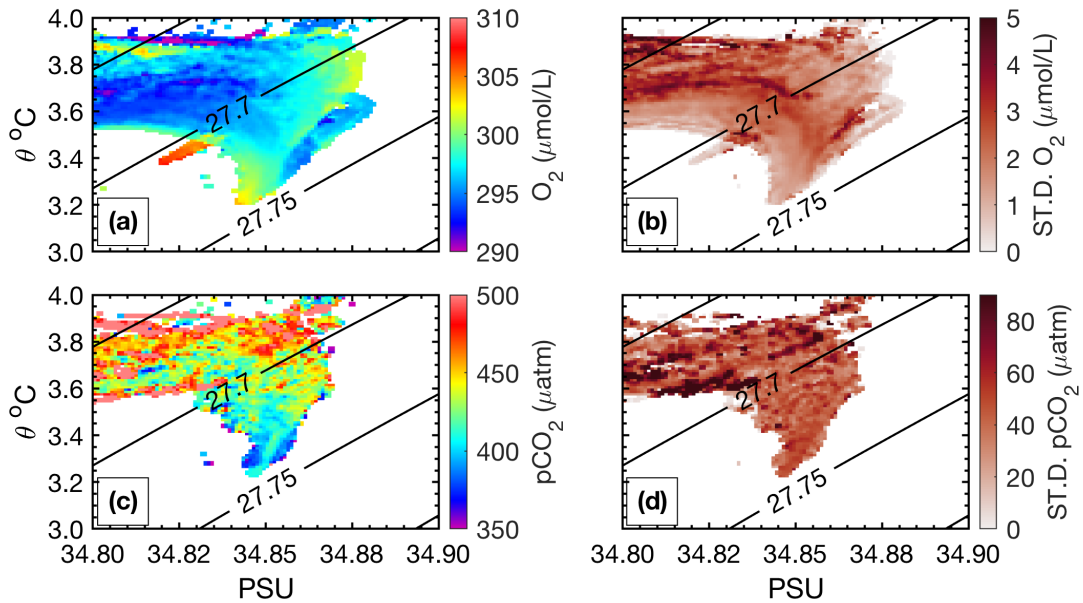
Figure 5.7: T–S diagram with isopycnal contours (σ_0) as black lines, color-coded for (a) intermediate depth O_2 and (c) pCO_2 observations and sample standard deviation (b) and (d) for each bin of O_2 and pCO_2 observations respectively.

5.3   Oxygen Content and AOU

The VITALS glider mission achieved an average resolution of 3 km in space and between 1.5 to 3 days in time for O_2 profiles. The calibration exercises and in-situ corrections with SeaCycler looked at the anomalies between platforms. Here we investigate gradients and fluxes in O_2 water column content over time in the spatial region. We compare O_2 profiles with solubility and look at the spatial differences between these two over time.

Two general layers exist in the observed region: a surface layer and an intermediate depth layer divided a by a weakening (eroding) mixed layer boundary. The surface layer is loosely coupled to the intermediate depth water layer but responds to storms
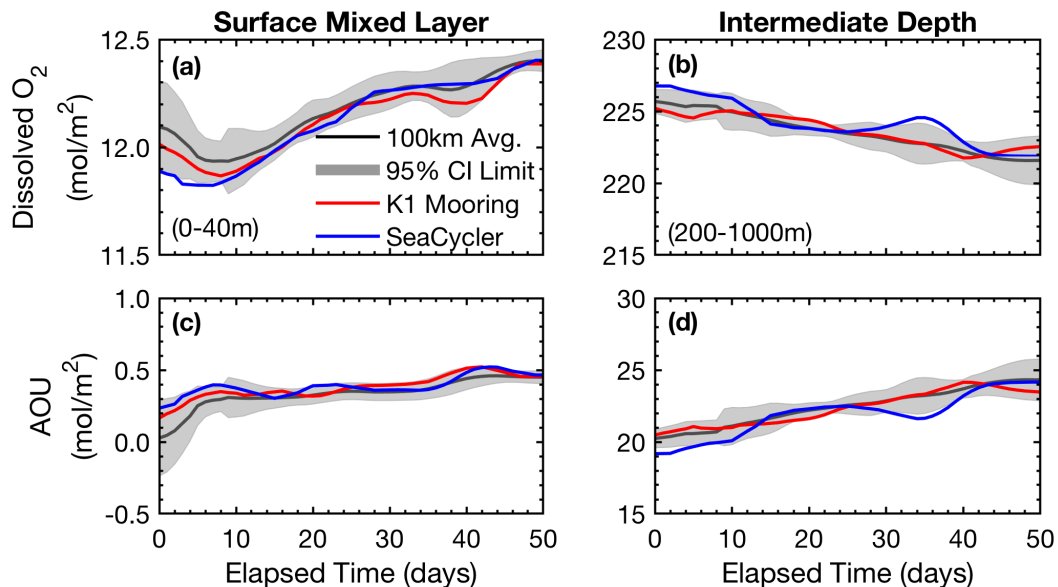
Figure 5.8: Panels (a) and (b) show column integrated O_2 and panels (c) and (d) AOU. Left panels show surface mixed layer (0–40 m) and right panels the intermediate depth layer (200–1000 m). Period shown (50 days) is the data record from 3 October to 22 November, 2016.

and surface atmospheric forcing within several days. However, the subsurface layer is slower to respond, more on a 3 to 14-day scale and propagation of high energy events are significantly dampened by this boundary. We make this distinction and divide the water layer here into two portions: a surface layer from 0 to 40 m depth, which is entirely mixed and nearly homogeneous, and the intermediate depth layer, which is also nearly homogeneous due to the characteristic Labrador Sea intermediate depth water low stratification (Clarke and Gascard, 1983). The homogeneity suggests O_2 content is nearly constant with depth in these two regimes. By integrating O_2 across

these layers, we estimate the total O_2 budget in mol·m^2.

$$\sum O_2 = \int_{h_1}^{h_2} [O_2] dz \tag{5.5}$$

Of interest to us is the biogenic influence on O_2 concentrations. Therefore, we remove the solubility controlled O_2 concentrations, following Wolf (2017), using the definition for O_2 solubility from Benson and Krause (1984), modified by Garcia and Gordon (1992).

$$AOU = [O_{2,\text{sol}}] - [O_2] \tag{5.6}$$

From the results in Figure 5.8, we see evidence of continuous loss of O_2, or undersaturation over the entire observation period by the glider with low spatial variability. This under-saturation is very pronounced towards the later fall as storm activity picks up. However, mixing alone is not the only driver of oxygen saturation. The SeaCycler record (Figure 4.5) clearly shows the biological productivity from August to October and increasing storminess later in the fall. It is likely that biogenic activity continues into the later fall/early winter in deeper waters and contributes to undersaturation even as storms increase vertical mixing and the exchange of O_2 between the surface and intermediate depth waters. O_2 under-saturation in intermediate depth water also agrees with results from Körtzinger et al. (2008). According to Koelling et al. (2017), this steep solubility gradient increases the strength of the O_2 uptake during the winter convection period. In the surface mixed layer, we see marginal oversaturation, followed by a period of weak undersaturation. The O_2 levels themselves take a noticeable dip in the surface layer in the first 10 days of the observation record, while the subsurface layer shows a continuous decrease in total O_2 content. The undersaturation of the intermediate depth layer in the fall with respect to solubility is likely

impacted by the strong biogenic cycling between spring/summer surface productivity and the O_2 uptake by subsurface bacteria. With future improvements of CO_2 sensors, it will be desirable to compare subsurface saturation states of both gasses to predict and track the local sinks of O_2 and CO_2 during deep convection in the Labrador Sea.

Chapter 6

Summary and Conclusions

This thesis presented the hydrographic data and results of a new type of CO_2 sensor, from a glider deployment in the Labrador Sea as part of the Ventilations, Interactions and Transport across the Labrador Sea (VITALS) program in the Fall of 2016 and the results from calibration tests in Trinity Bay in 2018. The Trinity Bay tests improved knowledge on sensor calibration issues and sensor performance on gliders. We also presented new glider observing concepts such as the staircase mission and demonstrated their utility in minimizing the effects of thermal lag in photo-chemical sensors. In the Introduction, we presented three questions for this thesis, answers to which are necessary to improve the capability of global carbon observing systems. In this final chapter, we summarize our findings to address each question and comment on future work.

6.1   Glider-based CO_2 Observing

We began the thesis and ensuing discussion by pointing towards the importance of measuring CO_2 in the ocean environment, and the essential role gliders can play in closing some of the observational gaps currently faced by those seeking to improve models and ecosystem projections either for the coastal or open ocean environment. Gliders as a platform for carbon observations have many benefits, but also significant challenges, as discussed in Section 2.4. The VITALS mission saw the first glider based deployment of the prototype CO_2 optode by Aanderaa Data Instruments. The sensor showed steady drift in the first cycle of the deployment and exhibited different response-time characteristics in standard glider profiling modes. The short answer is that this sensor does not offer the required reliability required for glider based carbon observing. Unique staircase missions and further testing of the sensor on a glider improved our knowledge on the sensor in glider applications, but more work would be required to find an equation or model that could correct for the long response time constant between changes in ambient conditions and sensor response. However, without further design improvements to the sensor and the foil chemistry, such correction is not generally feasible as there are currently three temperature-dependent and coupled processes that all contribute in a non-linear fashion to the final response time of the sensor.

Based on the CO_2 sensor performance discussion from Chapter 4 and the many issues with the current foil design one would arguably ask if there are not better alternatives available to date for glider based CO_2 monitoring than the Aanderaa CO_2 Optode. The answer is not straightforward and as Chapter 2 points out, many dif-

ferent variables must be considered before identifying a definite candidate for a glider sensor that could replace the current optode model tested in this thesis. The optode has key strengths: small size and low power consumption. If the foil stability and sensitivity can be improved, while also decreasing equilibration time from minutes to seconds, the sensor could become a desirable candidate for ocean gas measurements similar to the O_2 optode by the same manufacturer. The work by Saba et al. (2018), testing the ISFET pH sensor on a glider has shown promising results. Together with Alkalinity-Salinity relationships, one can resolve other CO_2 system parameters. Low drift, high stability and excellent power consumption make this sensor very attractive. It is likely that if the demand for this technology is proven to the manufacturer (Sea Bird), this sensor could soon be commercialized and released to the scientific community for purchase. Adapting the ISFET technology for gliders would have a significant impact on the ability of research groups to describe the space-time scales of CO_2 exchange with the atmosphere and ocean ecosystem impact of increasing anthropogenic CO_2 emissions into the atmosphere accurately. Bringing this technology to fruition is essential in a remote region such as the Labrador Sea where atmospheric changes interact with the deep ocean on time scales of years as supposed to decades. We are planning further deployments into the Labrador Sea to monitor changes in this environment as part of ongoing scientific projects involving research groups across Canada. We hope the ISFET technology will become available to the glider community soon to allow further exploration of the complex CO_2 linkages between the Labrador Sea and the rest of the global ocean.

6.2 Multi-Platform in-situ Data Corrections

The VITALS 2016 Labrador Sea SeaCycler–Glider deployment demonstrated the success of capitalizing on the strength of multiple observing platforms to improve the data quality of mobile platforms such as gliders. Strategies to mimic traditional sensor calibration procedures utilized by research ships were successfully demonstrated as was the capability to synchronize and synthesize data from different autonomous sensors and systems to achieve a coherent space-time data set. Our correction attempts for the experimental glider CO_2 optode, using other sensor instruments on a vertical profiler mooring (SeaCycler) were somewhat successful in calibrating the data set, but the data remained noisy. For the more reliable O_2 optode, this method worked well, and agreement in data after correction to within ± 10 μmol/L was achieved. The cross-platform in-situ corrected data set allowed for interesting comparisons across space and time observations. This is an important stepping stone to meet future observing mission requirements as ship time is becoming more challenging to access by research groups around the world. This in-situ referencing method for glider using other moorings and other platforms will become increasingly necessary as new types of measurements are being made with gliders and sensor technology that is still catching up in reliability to those that can are deployed from ships or moorings. Improvements in data transfer rates and direct communication between platforms could automate this process, improving data reliability in the future.

6.3   Labrador Sea Glider Observations

This thesis described and demonstrated new methods to reach the Labrador Sea from the coast without the use of a significant ship-time for both launch and recovery. Furthermore the collected data, shows that gliders can successfully be used to resolve some of the time and spatial scales that are in agreement with previous work in this region and point towards smaller scale energies not previously resolved by moorings or ship cruises. The Labrador Sea is a dynamic ocean frontier, and throughout the previous chapters, we underlined this message with observations, analysis and references to the literature. Through spectral analysis as well as correlation analysis, we showed the importance of resolving short time and spatial scales in the central Labrador Sea. Throughout the discussion in Chapter 5, we mention the issues around data resolution and challenges with gliders to resolve both spatial and temporal variability. In Chapter 3, we also described the technical issues of using gliders to observe the Labrador Sea due to its remote location.

One of the essential challenges encountered in this thesis and other glider missions is the issues of the spatial and temporal gaps. In the VITALS mission, a single glider was used to do repeat transects to observe a 100 km long track line every 3 days. This led to significant problems resolving smaller scale events such as submesoscale eddies referenced in the literature. In the future, the use of multiple gliders could potentially further reduce the spatial and temporal gaps. Having several gliders perform the same transect, slightly displaced from each other could result in shorter time and spatial differences between repeated measurements. Several gliders would improve resolution and linked to mooring data could allow for 3-dimensional budget estimation

of atmospheric exchange, vertical and lateral mixing and transport terms. Another issue with present observing capability is the lack of atmospheric measurements at sea. Wind speed, air temperature, heat flux - these are all critical components to describe deep convection in the Labrador Sea accurately. Surface crafts such as the Sailbuoy (manufactured by Offshore Sensing AS, Norway) have already demonstrated their ability to collect synoptic data in harsh environments such as the Norwegian sea in the winter. It is feasible that in the future, together with moorings and gliders, this vehicle could be deployed into the Labrador Sea to improve in-situ observations in the harsh winter-spring period.

Bibliography

Aagaard, K. and Carmack, E. C. (1989). The role of sea ice and other fresh water in the Arctic circulation. *Journal of Geophysical Research: Oceans*, 94(C10):14485–14498.

Adkins, J. F., Cheng, H., Boyle, E. A., Druffel, E. R., and Edwards, R. L. (1998). Deep-sea coral evidence for rapid change in ventilation of the deep North Atlantic 15,400 years ago. *Science*, 280(5364):725–728.

Alvarez, A. and Mourre, B. (2012). Optimum sampling designs for a glider–mooring observing network. *Journal of Atmospheric and Oceanic Technology*, 29(4):601–612.

Ardyna, M., Babin, M., Gosselin, M., Devred, E., Rainville, L., and Tremblay, J.-É. (2014). Recent Arctic Ocean sea ice loss triggers novel fall phytoplankton blooms. *Geophysical Research Letters*, 41(17):6207–6212.

Arrhenius, S. (1889). Über die Dissociationswärme und den Einfluss der Temperatur auf den Dissociationsgrad der Elektrolyte. *Zeitschrift fr Physikalische Chemie*, 4(1).

Arrigo, K. R., van Dijken, G. L., Castelao, R. M., Luo, H., Rennermalm, Å. K., Tedesco, M., Mote, T. L., Oliver, H., and Yager, P. L. (2017). Melting glaciers

stimulate large summer phytoplankton blooms in southwest Greenland waters. *Geophysical Research Letters*, 44(12):6278–6285.

Atamanchuk, D., Kononets, M., Thomas, P. J., Hovdenes, J., Tengberg, A., and Hall, P. O. (2015). Continuous long-term observations of the carbonate system dynamics in the water column of a temperate fjord. *Journal of Marine Systems*, 148:272–284.

Atamanchuk, D., Tengberg, A., Thomas, P. J., Hovdenes, J., Apostolidis, A., Huber, C., and Hall, P. O. (2014). Performance of a lifetime-based optode for measuring partial pressure of carbon dioxide in natural waters. *Limnology and Oceanography: Methods*, 12(2):63–73.

Avsic, T., Karstensen, J., Send, U., and Fischer, J. (2006). Interannual variability of newly formed Labrador Sea Water from 1994 to 2005. *Geophysical Research Letters*, 33(21).

Azetsu-Scott, K., Clarke, A., Falkner, K., Hamilton, J., Jones, E. P., Lee, C., Petrie, B., Prinsenberg, S., Starr, M., and Yeats, P. (2010). Calcium carbonate saturation states in the waters of the Canadian Arctic Archipelago and the Labrador Sea. *Journal of Geophysical Research: Oceans*, 115(C11).

Bailey, D. A., Rhines, P. B., and Häkkinen, S. (2005). Formation and pathways of North Atlantic Deep Water in a coupled ice–ocean model of the Arctic–North Atlantic Oceans. *Climate dynamics*, 25(5):497–516.

Bakker, D. C. E., Pfeil, B., Landa, C. S., Metzl, N., O'Brien, K. M., Olsen, A., Smith, K., et al. (2016). A multi-decade record of high-quality fCO$_2$ data in version 3 of the Surface Ocean CO$_2$ Atlas (SOCAT). *Earth System Science Data*, 8(2):383–413.

Beaton, A. D., Wadham, J. L., Hawkings, J., Bagshaw, E. A., Lamarche-Gagnon, G., Mowlem, M. C., and Tranter, M. (2017). High-resolution in situ measurement of nitrate in runoff from the Greenland Ice Sheet. *Environmental science & technology*, 51(21):12518–12527.

Bell, T., Briggs, R., Bachmayer, R., and Li, S. (2014). Augmenting Inuit knowledge for safe sea-ice travelThe SmartICE information system. In *2014 Oceans–St. John's*, pages 1–9. IEEE.

Benson, B. B. and Krause, D. (1984). The concentration and isotopic fractionation of oxygen dissolved in freshwater and seawater in equilibrium with the atmosphere. *Limnology and oceanography*, 29(3):620–632.

Bittig, H. C., Fiedler, B., Scholz, R., Krahmann, G., and Körtzinger, A. (2014). Time response of oxygen optodes on profiling platforms and its dependence on flow speed and temperature. *Limnology and Oceanography: Methods*, 12(8):617–636.

Bittig, H. C. and Körtzinger, A. (2015). Tackling oxygen optode drift: Near-surface and in-air oxygen optode measurements on a float provide an accurate in situ reference. *Journal of Atmospheric and Oceanic Technology*, 32(8):1536–1543.

Borges, A., Alin, S., Chavez, F., Vlahos, P., Johnson, K., Holt, J., Balch, W., Bates, N., Brainard, R., Cai, W., et al. (2010). A global sea surface carbon observing system: Inorganic and organic carbon dynamics in coastal oceans. *Proceedings of OceanObs'09: Sustained Ocean Observations and Information for Society*, 2.

Bresnahan, P. J., Martz, T. R., Takeshita, Y., Johnson, K. S., and Lashomb, M.

(2014). Best practices for autonomous measurement of seawater pH with the Honeywell Durafet. *Methods in Oceanography*, 9:44–60.

Brice-Bennett, C. (1992). *Obituary on the Labrador Coast Fishery.* The Committee on the Labrador Coast Fishery.

Broecker, W. S. (1991). The Great Ocean Conveyor. *Oceanography*, 4(2):79–89.

Broecker, W. S., Peteet, D. M., and Rind, D. (1985). Does the ocean–atmosphere system have more than one stable mode of operation? *Nature*, 315(6014):21.

Brunt, D. (1927). The period of simple vertical oscillations in the atmosphere. *Quarterly Journal of the Royal Meteorological Society*, 53(221):30–32.

Cairns, J. L. and Williams, G. O. (1976). Internal wave observations from a midwater float. *Journal of Geophysical Research*, 81(12):1943–1950.

Chanut, J., Barnier, B., Large, W., Debreu, L., Penduff, T., Molines, J. M., and Mathiot, P. (2008). Mesoscale eddies in the Labrador Sea and their contribution to convection and restratification. *Journal of Physical Oceanography*, 38(8):1617–1643.

Chatfield, C. (1998). *The Analysis of Time Series: An Introduction.* Chapman and Hall/CRC, 5 edition.

Clarke, J. S., Achterberg, E. P., Connelly, D. P., Schuster, U., and Mowlem, M. (2017a). Developments in marine pCO_2 measurement technology; towards sustained in situ observations. *TrAC Trends in Analytical Chemistry*, 88:53–61.

Clarke, J. S., Humphreys, M. P., Tynan, E., Kitidis, V., Brown, I., Mowlem, M., and Achterberg, E. P. (2017b). Characterization of a time-domain dual lifetime referencing pCO$_2$ optode and deployment as a high-resolution underway sensor across the high latitude North Atlantic Ocean. *Frontiers in Marine Science*, 4:396.

Clarke, R. A. (1984). Transport through the Cape Farewell – Flemish Cap section. Technical report, University of Iceland, Reykjavik.

Clarke, R. A. and Coote, A. (1988). The formation of Labrador Sea Water. Part III: The evolution of oxygen and nutrient concentration. *Journal of Physical Oceanography*, 18(3):469–480.

Clarke, R. A. and Gascard, J.-C. (1983). The formation of Labrador Sea water. Part I: Large-scale processes. *Journal of Physical Oceanography*, 13(10):1764–1778.

Clayton, T. D. and Byrne, R. H. (1993). Spectrophotometric seawater pH measurements: total hydrogen ion concentration scale calibration of m-cresol purple and at-sea results. *Deep Sea Research Part I: Oceanographic Research Papers*, 40(10):2115–2129.

Cohen, A. L. and Holcomb, M. (2009). Why corals care about ocean acidification: uncovering the mechanism. *Oceanography*, 22(4):118–127.

Cuny, J., Rhines, P. B., Niiler, P. P., and Bacon, S. (2002). Labrador Sea boundary currents and the fate of the Irminger Sea Water. *Journal of Physical Oceanography*, 32(2):627–647.

DeGrandpre, M., Hammar, T., Smith, S., and Sayles, F. (1995). In situ measurements of seawater pCO$_2$. *Limnology and Oceanography*, 40(5):969–975.

DeGrandpre, M., Körtzinger, A., Send, U., Wallace, D. W., and Bellerby, R. (2006). Uptake and sequestration of atmospheric CO$_2$ in the Labrador Sea deep convection region. *Geophysical Research Letters*, 33(21).

Denman, K. and Gargett, A. (1983). Time and space scales of vertical mixing and advection of phytoplankton in the upper ocean. *Limnology and oceanography*, 28(5):801–815.

deYoung, B., von Oppeln-Bronikowski, N., Matthews, R. B. J., and Bachmayer, R. (2018). Glider Operations in the Labrador Sea. *Journal of Ocean Technology*, 13(1).

Dickson, A. G. (1993). The measurement of seawater pH. *Marine Chemistry*, 44(2-4):131–142.

Dickson, R., Rudels, B., Dye, S., Karcher, M., Meincke, J., and Yashayaev, I. (2007). Current estimates of freshwater flux through Arctic and subarctic seas. *Progress in Oceanography*, 73(3-4):210–230.

Dickson, R. R., Meincke, J., Malmberg, S.-A., and Lee, A. J. (1988). The Great Salinity Anomaly in the northern North Atlantic 1968–1982. *Progress in Oceanography*, 20(2):103–151.

Dore, J. E., Lukas, R., Sadler, D. W., Church, M. J., and Karl, D. M. (2009). Physical and biogeochemical modulation of ocean acidification in the central North Pacific. *Proceedings of the National Academy of Sciences*, 106(30):12235–12240.

Ducklow, H. W., Doney, S. C., and Steinberg, D. K. (2009). Contributions of long-term research and time-series observations to marine ecology and biogeochemistry. *Annual Review of Marine Science*, 1:279–302.

Durkalec, A., Furgal, C., Skinner, M. W., and Sheldon, T. (2015). Climate change influences on environment as a determinant of Indigenous health: Relationships to place, sea ice, and health in an Inuit community. *Social science & medicine*, 136:17–26.

Eriksen, C. C., Osse, T. J., Light, R. D., Wen, T., Lehman, T. W., Sabin, P. L., Ballard, J. W., and Chiodi, A. M. (2001). Seaglider: A long-range autonomous underwater vehicle for oceanographic research. *IEEE Journal of oceanic Engineering*, 26(4):424–436.

Eriksen, C. C. and Rhines, P. (2008). Convective to Gyre-Scale Dynamics: Seaglider Campaigns in the Labrador Sea 2003–2005. In *Arctic–Subarctic Ocean Fluxes*, pages 613–628. Springer.

Fick, A. (1855). Über Diffusion. *Annalen der Physik*, 170(1):59–86.

Fiedler, B., Fietzek, P., Vieira, N., Silva, P., Bittig, H. C., and Körtzinger, A. (2013). In situ CO_2 and O_2 measurements on a profiling float. *Journal of Atmospheric and Oceanic Technology*, 30(1):112–126.

Fiorelli, E., Bhatta, P., Leonard, N. E., and Shulman, I. (2003). Adaptive sampling using feedback control of an autonomous underwater glider fleet. In *Proceedings of 13th Int. Symp. on Unmanned Untethered Submersible Technology (UUST)*, pages 1–16.

Fischer, J., Schott, F. A., and Dengler, M. (2004). Boundary circulation at the exit of the Labrador Sea. *Journal of Physical Oceanography*, 34(7):1548–1570.

Fontela, M., García-Ibáñez, M. I., Hansell, D. A., Mercier, H., and Pérez, F. F. (2016). Dissolved organic carbon in the North Atlantic Meridional Overturning Circulation. *Scientific reports*, 6:26931.

Frajka-Williams, E. (2009). *The Spring Phytoplankton Bloom and Vertical Velocities in the Stratified and Deep Convecting Labrador Sea, as Observed by Seagliders*. PhD thesis, University of Washington.

Frajka-Williams, E., Rhines, P. B., and Eriksen, C. C. (2009). Physical controls and mesoscale variability in the Labrador Sea spring phytoplankton bloom observed by Seaglider. *Deep Sea Research Part I: Oceanographic Research Papers*, 56(12):2144–2161.

Frajka-Williams, E., Rhines, P. B., and Eriksen, C. C. (2014). Horizontal stratification during deep convection in the Labrador Sea. *Journal of Physical Oceanography*, 44(1):220–228.

Fritzsche, E., Gruber, P., Schutting, S., Fischer, J. P., Strobl, M., Müller, J. D., Borisov, S. M., and Klimant, I. (2017). Highly sensitive poisoning-resistant optical carbon dioxide sensors for environmental monitoring. *Analytical Methods*, 9(1):55–65.

Fritzsche, E., Staudinger, C., Fischer, J. P., Thar, R., Jannasch, H. W., Plant, J. N., Blum, M., Massion, G., Thomas, H., Hoech, J., et al. (2018). A validation and

comparison study of new, compact, versatile optodes for oxygen, pH and carbon dioxide in marine environments. *Marine Chemistry*, 207:63–76.

Garau, B., Ruiz, S., Zhang, W. G., Pascual, A., Heslop, E., Kerfoot, J., and Tintoré, J. (2011). Thermal lag correction on Slocum CTD glider data. *Journal of Atmospheric and Oceanic Technology*, 28(9):1065–1071.

Garcia, H. E. and Gordon, L. I. (1992). Oxygen solubility in seawater: Better fitting equations. *Limnology and oceanography*, 37(6):1307–1312.

Garrett, C. and Munk, W. (1975). Space-time scales of internal waves: A progress report. *Journal of Geophysical Research*, 80(3):291–297.

Gascard, J.-C. (1973). Vertical motions in a region of deep water formation. In *Deep Sea Research and Oceanographic Abstracts*, volume 20, pages 1011–1027. Elsevier.

Gascard, J.-C. and Clarke, R. A. (1983). The formation of Labrador Sea Water. Part II. Mesoscale and smaller-scale processes. *Journal of Physical Oceanography*, 13(10):1779–1797.

Goff, J. A. (1957). Saturation pressure of water on the new Kelvin temperature scale. *Transactions of the American society of heating and ventilating engineers*, pages 347–354.

Goodin, W. R., McRae, G. J., and Seinfeld, J. H. (1979). A Comparison of Interpolation Methods for Sparse Data: Application to Wind and Concentration Fields. *Journal of Applied Meteorology (1962-1982)*, 18(6):761–771.

Guinotte, J. and Fabry, V. J. (2009). The threat of acidification to ocean ecosystems. *Ocean acidificationfrom ecological impacts to policy Opportunities*, 25(1):2.

Hátún, H., Eriksen, C. C., and Rhines, P. B. (2007). Buoyant eddies entering the Labrador Sea observed with gliders and altimetry. *Journal of Physical Oceanography*, 37(12):2838–2854.

Hauri, C., McDonnell, A. M., Winsor, P., Irving, B., and Statscewich, H. (2018). *Development of an Autonomous Carbon Glider to Monitor Sea-air CO_2 Fluxes in the Chukchi Sea*. Coastal Marine Institute, College of Fisheries and Ocean Sciences.

Howatt, T., Palter, J. B., Robin Matthews, J. B., deYoung, B., Bachmayer, R., and Claus, B. (2018). Ekman and Eddy Exchange of Freshwater and Oxygen across the Labrador Shelf Break. *Journal of Physical Oceanography*, 48(5):1015–1031.

Jähne, B., Heinz, G., and Dietrich, W. (1987). Measurement of the diffusion coefficients of sparingly soluble gases in water. *Journal of Geophysical Research: Oceans*, 92(C10):10767–10776.

Jiang, Z.-P., Hydes, D. J., Hartman, S. E., Hartman, M. C., Campbell, J. M., Johnson, B. D., Schofield, B., Turk, D., Wallace, D., Burt, W. J., et al. (2014). Application and assessment of a membrane-based pCO_2 sensor under field and laboratory conditions. *Limnology and Oceanography: Methods*, 12(4):264–280.

Johnson, K. S., Berelson, W. M., Boss, E. S., Chase, Z., Claustre, H., Emerson, S. R., Gruber, N., Körtzinger, A., Perry, M. J., and Riser, S. C. (2009). Observing biogeochemical cycles at global scales with profiling floats and gliders: prospects for a global array. *Oceanography*, 22(3):216–225.

Johnson, K. S., Jannasch, H. W., Coletti, L. J., Elrod, V. A., Martz, T. R., Takeshita, Y., Carlson, R. J., and Connery, J. G. (2016). Deep-Sea DuraFET: A pressure tolerant pH sensor designed for global sensor networks. *Analytical chemistry*, 88(6):3249–3256.

Johnson, K. S., Plant, J. N., Coletti, L. J., Jannasch, H. W., Sakamoto, C. M., Riser, S. C., Swift, D. D., Williams, N. L., Boss, E., Haëntjens, N., et al. (2017). Biogeochemical sensor performance in the SOCCOM profiling float array. *Journal of Geophysical Research: Oceans*, 122(8):6416–6436.

Katsman, C. A., Spall, M. A., and Pickart, R. S. (2004). Boundary current eddies and their role in the restratification of the Labrador Sea. *Journal of Physical Oceanography*, 34(9):1967–1983.

Khatiwala, S., Tanhua, T., Mikaloff Fletcher, S., Gerber, M., Doney, S., Graven, H., Gruber, N., McKinley, G., Murata, A., Ríos, A., et al. (2013). Global ocean storage of anthropogenic carbon. *Biogeosciences*, 10(4):2169–2191.

Kieke, D., Rhein, M., Stramma, L., Smethie, W. M., Bullister, J. L., and LeBel, D. A. (2007). Changes in the pool of Labrador Sea Water in the subpolar North Atlantic. *Geophysical Research Letters*, 34(6).

Koelling, J., Wallace, D. W., Send, U., and Karstensen, J. (2017). Intense oceanic uptake of oxygen during 2014–2015 winter convection in the Labrador Sea. *Geophysical Research Letters*, 44(15):7855–7864.

Körtzinger, A., Schimanski, J., Send, U., and Wallace, D. (2004). The ocean takes a deep breath. *Science*, 306(5700):1337–1337.

Körtzinger, A., Send, U., Wallace, D. W., Karstensen, J., and DeGrandpre, M. (2008). Seasonal cycle of O_2 and pCO_2 in the central Labrador Sea: Atmospheric, biological, and physical implications. *Global Biogeochemical Cycles*, 22(1).

Lacis, A. A., Schmidt, G. A., Rind, D., and Ruedy, R. A. (2010). Atmospheric CO_2: Principal control knob governing Earth's temperature. *Science*, 330(6002):356–359.

Landschützer, P. (2014). *Variability of the Global Ocean Carbon Sink (1998 through 2011)*. PhD thesis, University of East Anglia.

Landschützer, P., Gruber, N., Bakker, D., and Schuster, U. (2014). Recent variability of the global ocean carbon sink. *Global Biogeochemical Cycles*, 28(9):927–949.

Lavender, K. L., Davis, R. E., and Owens, W. B. (2002). Observations of open-ocean deep convection in the Labrador Sea from subsurface floats. *Journal of Physical Oceanography*, 32(2):511–526.

Lazier, J. (1973). The renewal of Labrador Sea water. In *Deep Sea Research and Oceanographic Abstracts*, volume 20, pages 341–353. Elsevier.

Lazier, J. and Wright, D. (1993). Annual velocity variations in the Labrador Current. *Journal of Physical Oceanography*, 23(4):659–678.

Lazier, J. R. (1980). Oceanographic conditions at ocean weather ship Bravo, 1964–1974. *Atmosphere-ocean*, 18(3):227–238.

Le Quéré, C., Moriarty, R., Andrew, R. M., Canadell, J. G., Sitch, S., Korsbakken, J. I., Friedlingstein, P., Peters, G. P., Andres, R. J., Boden, T. A., et al. (2015). Global carbon budget 2015. *Earth System Science Data*, 7:349–396.

Lewis, E., Wallace, D., and Allison, L. J. (1998). Program Developed for CO_2 System Calculations. Technical report, Brookhaven National Laboratory, Department of Applied Science, Upton, NY (United States).

Lilly, J. M. and Rhines, P. B. (2002). Coherent Eddies in the Labrador Sea Observed from a Mooring. *Journal of Physical Oceanography*, 32(2):585–598.

Lilly, J. M., Rhines, P. B., Schott, F., Lavender, K., Lazier, J., Send, U., and D'Asaro, E. (2003). Observations of the Labrador Sea eddy field. *Progress in Oceanography*, 59(1):75–176.

Lilly, J. M., Rhines, P. B., Visbeck, M., Davis, R., Lazier, J. R., Schott, F., and Farmer, D. (1999). Observing deep convection in the Labrador Sea during winter 1994/95. *Journal of Physical Oceanography*, 29(8):2065–2098.

Lozier, M., Li, F., Bacon, S., Bahr, F., Bower, A., Cunningham, S., de Jong, M., de Steur, L., Fischer, J., Gary, S., et al. (2019). A sea change in our view of overturning in the subpolar North Atlantic. *Science*, 363(6426):516–521.

Lumpkin, R. and Speer, K. (2003). Large-scale vertical and horizontal circulation in the North Atlantic Ocean. *Journal of Physical Oceanography*, 33(9):1902–1920.

Malmberg, S. A. (1969). Hydrographic changes in the waters between Iceland and Jan Mayen in the last decade. *Jökull*.

Marshall, J. and Schott, F. (1999). Open-ocean convection: Observations, theory, and models. *Reviews of Geophysics*, 37(1):1–64.

Martz, T. R., Connery, J. G., and Johnson, K. S. (2010). Testing the Honeywell Durafet® for seawater pH applications. *Limnology and Oceanography: Methods*, 8(5):172–184.

McDougall, T. J. and Barker, P. M. (2011). Getting started with TEOS-10 and the Gibbs Seawater (GSW) oceanographic toolbox. *SCOR/IAPSO WG*, 127:1–28.

Mesinger, F., DiMego, G., Kalnay, E., Mitchell, K., Shafran, P. C., Ebisuzaki, W., Jović, D., Woollen, J., Rogers, E., Berbery, E. H., et al. (2006). North American Regional Reanalysis. *Bulletin of the American Meteorological Society*, 87(3):343–360.

Miller, C. A., Pocock, K., Evans, W., and Kelley, A. L. (2018). An evaluation of the performance of Sea-Bird Scientific's SeaFET™ autonomous pH sensor: considerations for the broader oceanographic community. *Ocean Science*, 14(4):751–768.

Millero, F. J. (2007). The Marine Inorganic Carbon Cycle. *Chemical reviews*, 107(2):308–341.

Moore, G., Pickart, R. S., and Renfrew, I. A. (2008). Buoy observations from the windiest location in the world ocean, Cape Farewell, Greenland. *Geophysical Research Letters*, 35(18).

Morison, J., Andersen, R., Larson, N., D'Asaro, E., and Boyd, T. (1994). The correction for thermal-lag effects in Sea-Bird CTD data. *Journal of atmospheric and oceanic technology*, 11(4):1151–1164.

Murray, G., Neis, B., and Schneider, D. C. (2007). Lessons from a Multi-Scale Histori-

cal Reconstruction of Newfoundland and Labrador Fisheries. *Coastal Management*, 36(1):81–108.

Nightingale, P. D., Liss, P. S., and Schlosser, P. (2000). Measurements of air-sea gas transfer during an open ocean algal bloom. *Geophysical Research Letters*, 27(14):2117–2120.

Okazaki, R. R., Sutton, A. J., Feely, R. A., Dickson, A. G., Alin, S. R., Sabine, C. L., Bunje, P. M., and Virmani, J. I. (2017). Evaluation of marine pH sensors under controlled and natural conditions for the Wendy Schmidt Ocean Health X-PRIZE. *Limnology and Oceanography: Methods*, 15(6):586–600.

Osse, T. J. and Eriksen, C. C. (2007). The Deepglider: A full ocean depth glider for oceanographic research. In *OCEANS 2007*, pages 1–12. IEEE.

Parkinson, C. L. (2000). Variability of Arctic sea ice: The view from space, an 18-year record. *Arctic*, pages 341–358.

Peeters, F., Atamanchuk, D., Tengberg, A., Encinas-Fernández, J., and Hofmann, H. (2016). Lake metabolism: Comparison of lake metabolic rates estimated from a diel CO_2 and the common diel O_2 technique. *PloS one*, 11(12):e0168393.

Pickart, R. S., Torres, D. J., and Clarke, R. A. (2002). Hydrography of the Labrador Sea during active convection. *Journal of Physical Oceanography*, 32(2):428–457.

Prinsenberg, S., Peterson, I., Narayanan, S., and Umoh, J. (1997). Interaction between atmosphere, ice cover, and ocean off Labrador and Newfoundland from 1962 to 1992. *Canadian Journal of Fisheries and Aquatic Sciences*, 54(S1):30–39.

Pro-Oceanus Systems Inc. (2018). *CO_2-Pro CV User Manual.* 80 Pleasant Street, Bridgewater, Nova Scotia, Canada, B4V 1N1, 4th edition.

Pro-Oceanus Systems Inc. (2019). *MINI $CO_2{}^{TM}$.* 80 Pleasant Street, Bridgewater, Nova Scotia, Canada, B4V 1N1.

Robe, R., Maier, D., and Russell, W. (1980). Long-term drift of icebergs in Baffin Bay and the Labrador Sea. *Cold Regions Science and Technology*, 1(3-4):183–193.

Rudnick, D. L. (2016). Ocean research enabled by underwater gliders. *Annual Review of Marine Science*, 8:519–541.

Rudnick, D. L., Davis, R. E., Eriksen, C. C., Fratantoni, D. M., and Perry, M. J. (2004). Underwater gliders for ocean research. *Marine Technology Society Journal*, 38(2):73–84.

Russell, J., Sarmiento, J., Cullen, H., Hotinski, R., Johnson, K., Riser, S., and Talley, L. (2014). The Southern Ocean Carbon and Climate Observations and Modeling Program (SOCCOM). *Ocean Carbon Biogeochem. Newsl*, 7:1–5.

Saba, G. K., Wright-Fairbanks, E., Miles, T. N., Chen, B., Cai, W.-J., Wang, K., Barnard, A. H., Branham, C. W., and Jones, C. P. (2018). Developing a profiling glider pH sensor for high resolution coastal ocean acidification monitoring. In *OCEANS 2018 MTS/IEEE Charleston*, pages 1–8. IEEE.

Sabine, C. L., Feely, R. A., Gruber, N., Key, R. M., Lee, K., Bullister, J. L., Wanninkhof, R., Wong, C., Wallace, D. W., Tilbrook, B., et al. (2004). The oceanic sink for anthropogenic CO_2. *science*, 305(5682):367–371.

Sabine, C. L. and Tanhua, T. (2010). Estimation of anthropogenic CO_2 inventories in the ocean. *Annual review of marine science*, 2:175–198.

Sarmiento, J. L. (2006). *Ocean Biogeochemical Dynamics*. Princeton University Press, Princeton, N.J.

Sarmiento, J. L. and Gruber, N. (2002). Sinks for anthropogenic carbon. *Physics today*, 55(8):30–36.

Sathiyamoorthy, S. and Moore, G. (2002). Buoyancy flux at ocean weather station Bravo. *Journal of Physical Oceanography*, 32(2):458–474.

Schillinger, D. J., deYoung, B., and Foley, J. S. (2000). Physical and Biological Tow-Yo Data from Trinity Bay, July 2000. Technical report, Memorial University.

Schledermann, P. (1980). Polynyas and prehistoric settlement patterns. *Arctic*, pages 292–302.

Send, U., Fowler, G., Siddall, G., Beanlands, B., Pittman, M., Waldmann, C., Karstensen, J., and Lampitt, R. (2013). SeaCycler: A moored open-ocean profiling system for the upper ocean in extended self-contained deployments. *Journal of Atmospheric and Oceanic Technology*, 30(7):1555–1565.

Sherwood, O. A. and Edinger, E. N. (2009). Ages and growth rates of some deep-sea gorgonian and antipatharian corals of Newfoundland and Labrador. *Canadian Journal of Fisheries and Aquatic Sciences*, 66(1):142–152.

Stirling, I. (1980). The biological importance of polynyas in the Canadian Arctic. *Arctic*, pages 303–315.

Stommel, H. et al. (1989). The Slocum Mission. *Oceanography*, 2(1):22–25.

Stouffer, R. J., Yin, J., Gregory, J., Dixon, K., Spelman, M., Hurlin, W., Weaver, A., Eby, M., Flato, G., Hasumi, H., et al. (2006). Investigating the causes of the response of the Thermohaline Circulation to past and future climate changes. *Journal of Climate*, 19(8):1365–1387.

Sudom, D., Timco, G., Sand, B., and Fransson, L. (2011). Analysis of first-year and old ice ridge characteristics. In *International Conference on Port and Ocean Engineering under Arctic Conditions: 10/07/2011–14/07/2011*.

Takahashi, T., Sutherland, S. C., Sweeney, C., Poisson, A., Metzl, N., Tilbrook, B., Bates, N., Wanninkhof, R., Feely, R. A., Sabine, C., et al. (2002). Global sea–air CO_2 flux based on climatological surface ocean pCO_2, and seasonal biological and temperature effects. *Deep Sea Research Part II: Topical Studies in Oceanography*, 49(9-10):1601–1622.

Takeshita, Y., Martz, T. R., Johnson, K. S., and Dickson, A. G. (2014). Characterization of an ion sensitive field effect transistor and chloride ion selective electrodes for pH measurements in seawater. *Analytical chemistry*, 86(22):11189–11195.

Testor, P., deYoung, B., Rudnick, D., Glenn, S., Hayes, D., Lee, C. M., Pattiaratchi, C., Hill, K., Heslop, E., Turpin, V., et al. (2019). Ocean Gliders: a component of the integrated GOOS. in review.

Testor, P., Meyers, G., Pattiaratchi, C., Bachmayer, R., Hayes, D., Pouliquen, S., Petit de la Villeon, L., Carval, T., Ganachaud, A., Gourdeau, L., et al. (2010).

Gliders as a component of future observing systems. *Proceedings of OceanObs'09: Sustained Ocean Observations and Information for Society*, 2.

Tittensor, D. P., deYoung, B., and Foley, J. S. (2002). Analysis of Physical Oceanographic Data from Trinity Bay, May-August 2002. Technical report, Memorial University.

Trivett, N., Hudec, V., and Wong, C. (1994). Atmospheric Carbon Dioxide (CO_2) Records from Sites in the AES Air Sampling Network.

Uchida, H., Kawano, T., Kaneko, I., and Fukasawa, M. (2008). In situ calibration of optode-based oxygen sensors. *Journal of Atmospheric and Oceanic Technology*, 25(12):2271–2281.

Väisäla, V. (1925). Über die Wirkung der Windschwankungen auf die Pilot beobachtungen. *Soc. Sci. Fennica, Commentationes Phys.-Math. II*, 19:37.

van Aken, H. M., de Jong, M. F., and Yashayaev, I. (2011). Decadal and multidecadal variability of Labrador Sea Water in the north-western North Atlantic Ocean derived from tracer distributions: Heat budget, ventilation, and advection. *Deep Sea Research Part I: Oceanographic Research Papers*, 58(5):505–523.

van Heuven, S. M., Hoppema, M., Jones, E. M., and de Baar, H. J. (2014). Rapid invasion of anthropogenic CO_2 into the deep circulation of the Weddell Gyre. *Philosophical Transactions of the Royal Society A: Mathematical, Physical and Engineering Sciences*, 372(2019):20130056.

Van Sebille, E., Baringer, M. O., Johns, W. E., Meinen, C. S., Beal, L. M., De Jong,

M. F., and Van Aken, H. M. (2011). Propagation pathways of classical Labrador Sea water from its source region to 26°N. *Journal of Geophysical Research: Oceans*, 116(C12).

Volk, T. and Hoffert, M. I. (1985). Ocean carbon pumps: Analysis of relative strengths and efficiencies in ocean-driven atmospheric CO_2 changes. *The carbon cycle and atmospheric CO_2: natural variations Archean to present*, pages 99–110.

Wallace, D. and Lazier, J. (1988). Anthropogenic chlorofluoromethanes in newly formed Labrador Sea Water. *Nature*, 332(6159):61.

Wanninkhof, R. (1992). Relationship between wind speed and gas exchange over the ocean. *Journal of Geophysical Research: Oceans*, 97(C5):7373–7382.

Wanninkhof, R. and McGillis, W. R. (1999). A cubic relationship between air-sea CO_2 exchange and wind speed. *Geophysical Research Letters*, 26(13):1889–1892.

Watson, A. J., Schuster, U., Bakker, D. C., Bates, N. R., Corbière, A., González-Dávila, M., Friedrich, T., Hauck, J., Heinze, C., Johannessen, T., et al. (2009). Tracking the variable North Atlantic sink for atmospheric CO_2. *Science*, 326(5958):1391–1393.

Weiss, R. F. (1974). Carbon dioxide in water and seawater: the solubility of a non-ideal gas. *Marine chemistry*, 2(3):203–215.

Wolf, M. (2017). Oxygen saturation surrounding deep-water formation events in the Labrador Sea from Argo-O_2 data. Master's thesis, University of Victoria, Canada.

Yao, W. and Byrne, R. H. (1998). Simplified seawater alkalinity analysis: Use of linear array spectrometers. *Deep Sea Research Part I: Oceanographic Research Papers*, 45(8):1383–1392.

Yashayaev, I. (2007). Hydrographic changes in the Labrador Sea, 1960–2005. *Progress in Oceanography*, 73(3-4):242–276.

Yashayaev, I. and Loder, J. W. (2009). Enhanced production of Labrador Sea water in 2008. *Geophysical Research Letters*, 36(1).

Zeebe, R. E., Ridgwell, A., and Zachos, J. C. (2016). Anthropogenic carbon release rate unprecedented during the past 66 million years. *Nature Geoscience*, 9(4):325.

Appendix A

Instrument Offsets

Table A.1 are the results from sensor testing at the Department of Fisheries and Oceans (DFO) in St. John's, Canada on August 27, 2018. Tests were conducted in a seawater basin 2.5 m deep. Oxygen was nearly 100% saturated with respect to the atmosphere. A reference CTD-Rosette system was immersed into the basin together with the glider, and reference CTD to compare instrument readings and take bottle samples of pCO_2 (DIC–pH conversion) and O_2 for calibration of optode sensors.

Table A.1: Instrument Calibration Offsets from Trinity Bay Tests.

Instrument	Serial	Manufacturer	Units	Accuracy	Variance	Mean Offset
SBE 19+ V2		Sea Bird Scientific	°C	0.005 (initial)	0.0742	0.0056
			S/m	0.0005 (initial)	0.0201	0.0123
Glider GPCT		Sea Bird Scientific	°C	0.0445	0.0445	-0.022
			S/m	0.0153	0.0153	-0.081
O_2 Optode (4831)	333	Aanderaa	μmol/L	$\pm$ 2	0.493	13.26
	124			(1.5% calibration range)	0.904	25.12
CO_2 Optode (4797)	56		μatm	Unknown	187.99	1969.83
	57				11.07	-461.14

Appendix B

MATLAB Code

Included here is select MATLAB® code pertaining to the CO_2 optode correction algorithms used to prepare the data shown in this thesis.

B.1 CO_2 Optode Time Fitting Algorithm

```
load('unit473_oxy.mat');
% time
t0 = gl.time-gl.time(1)*86400; % seconds

signal_raw = gl.pCO2_phase;
temp = gl.temp;
press = gl.press;

mask=isnan(signal_raw);
```

```
temp(mask)=[];
t0(mask)=[];
press(mask)=[];
signal_raw(mask)=[];


% setup model for fitting
fo = fitoptions('Method','NonlinearLeastSquares',...
                'StartPoint',[43 48 100]);
fo.MaxIter = 6000;
fo.MaxFunEvals = 1000;
fo.Upper = [100,100,1000];
fo.Lower = [0,0,0];
ft = fittype('(a-b)*exp(-x/tau)+b','independent',...
'x','options',fo);


% find segments
[pidx,pdir]=findProfiles(press,'STALL',10);
u_pidx=unique(pidx);
N_prof=length(u_pidx);


j = 0;
for i = 1:N_prof
    if (nanmean(pdir(pidx==u_pidx(i)))== 1 ...
```

```
    |  nanmean ( pdir ( pidx==u_pidx ( i )))== −1)
        if  length ( find ( pidx==u_pidx ( i ))) >100;

            j  =  j+1;

            z  =  press ( pidx==u_pidx ( i ));

            T  =  temp ( pidx==u_pidx ( i ));

            x  =  signal_raw ( pidx==u_pidx ( i ));

            t  =  t0 ( pidx==u_pidx ( i ));  t  =  t−t ( 1 );


            nan_flag  =  isnan ( x )  |  isnan (T)  |  isnan ( t );

            t ( nan_flag )=[];  x ( nan_flag )=[];

            T( nan_flag )=[];  z ( nan_flag )=[];

            [˜, id1]=min( abs (T−T( 1 )));

            T1=T( id1 );

            [˜, id2]=max( abs (T−T( 1 )));

            T2=T( id2 );

            dX( j )  =  x (end)−x ( 1 );

            if  z (end)−z(1)<0 % gaining  temperature  +

                x=flipud ( x );

            end

            [ f , gof , info ]  =  fit ( t ,x, ft , ’robust ’ , ’LAR’ );

            a ( j )  =  f . a ;

            b ( j )  =  f . b ;

            tau ( j )  =  f . tau ;
```

```
            dT( j )  =  T2–T1;

            dt ( j )  =  t (end)−t ( 1 );

            rmse ( j )  =  gof . rmse ;

        end

    end

end


% save  e−folding  scale  data  points
clear  ft ;
ft .dT = dT;
ft . rmse  =  rmse ;
ft . a  =  a ;
ft . b  =  b ;
ft . tau  =  tau ;
ft . dt  =  dt ;
ft .dX = dX;
save ( ' pCO2_fit_vitals_2016 ' , ' ft ' )
```

B.2   CO$_2$ Optode Response Time Correction

```
load ( ' unit473_oxy . mat ' ) ;
t0  =  gl . time−gl . time ( 1 )∗86400; % seconds
signal_raw  =  gl . pCO2_phase ;
temp_raw  =  gl . temp ;
```

```
press = gl.press;


% get well defined optode points
nan_flags = isnan(signal_raw) | isnan(temp_raw) | isnan(t0);
signal_raw(nan_flags) = [];
t0(nan_flags) = [];
temp_raw(nan_flags) = [];
load('vitals_fit.mat');


%alocate
N = length(signal_raw);
signal_c = zeros(N,1);
dTemp = zeros(N,1);
tau = zeros(N,1);
dt = zeros(N,1);


% initialize
signal_c(1) = signal_raw(1);


for i = 2:N;
    dt = t0(i)-t0(i-1);
    dTemp = temp_raw(i)-temp_raw(i-1);
    tau = ft.a*dTemp+ft.b;
```

```
    if  tau<0
        tau=abs(tau);
    end
    signal_c(i) = (signal_raw(i)-(signal_raw(i-1)*...
    exp(-dt/tau)))/(1-exp(-dt/tau));
end


pCO2 = NaN(length(gl.pCO2_phase),1);
pCO2(~nan_flags)=getpCO2_orig(signal_c,temp_raw)-1276;
pCO2_uc=getpco2_orig(gl.pCO2_phase,gl.temp)-1276;


gl.pCO2_uc = pCO2_uc; % uncorrected for response time
gl.pCO2 = pCO2;
save('unit473_optodes.mat','gl')
```